Earth and Planetary Science Letters 430 (2015) 115–128

Contents lists available at ScienceDirect

Earth and Planetary Science Letters

www.elsevier.com/locate/epsl

Pervasive remagnetization of detrital zircon host rocks in the Jack Hills, Western Australia and implications for records of the early geodynamo

Benjamin P. Weiss [a,b,*], Adam C. Maloof [c], Nicholas Tailby [d,e], Jahandar Ramezani [a], Roger R. Fu [a], Veronica Hanus [a], Dustin Trail [f], E. Bruce Watson [d,e], T. Mark Harrison [g], Samuel A. Bowring [a], Joseph L. Kirschvink [h,i], Nicholas L. Swanson-Hysell [b], Robert S. Coe [j]

[a] Department of Earth, Atmospheric, and Planetary Sciences, Massachusetts Institute of Technology, 77 Massachusetts Avenue, Cambridge, MA 02139, USA
[b] Department of Earth and Planetary Science, University of California (UC), Berkeley, Berkeley, CA 94720, USA
[c] Department of Geosciences, Princeton University, Guyot Hall, Washington Road, Princeton, NJ 08544, USA
[d] Department of Earth and Environmental Sciences, Rensselaer Polytechnic Institute, Troy, NY 12180, USA
[e] New York Center for Astrobiology, Rensselaer Polytechnic Institute, Troy, NY 12180, USA
[f] Department of Earth and Environmental Sciences, Box 270221, University of Rochester, Rochester, NY 14627, USA
[g] Institute of Geophysics and Planetary Physics, UC, Los Angeles, Los Angeles, CA 90095, USA
[h] Division of Geological and Planetary Sciences, California Institute of Technology, USA
[i] Earth-Life Science Institute, Tokyo Institute of Technology, Meguro, Tokyo, Japan
[j] Department of Earth and Planetary Sciences, UC, Santa Cruz, CA 95064, USA

ARTICLE INFO

Article history:
Received 11 May 2015
Received in revised form 29 July 2015
Accepted 30 July 2015
Available online xxxx
Editor: B. Buffett

Keywords:
geodynamo
paleointensity
core
Jack Hills
detrital zircons
Hadean earth

ABSTRACT

It currently is unknown when Earth's dynamo magnetic field originated. Paleomagnetic studies indicate that a field with an intensity similar to that of the present day existed 3.5 billion years ago (Ga). Detrital zircon crystals found in the Jack Hills of Western Australia are some of the very few samples known to substantially predate this time. With crystallization ages ranging from 3.0–4.38 Ga, these zircons might preserve a record of the missing first billion years of Earth's magnetic field history. However, a key unknown is the age and origin of magnetization in the Jack Hills zircons. The identification of >3.9 Ga (i.e., Hadean) field records requires first establishing that the zircons have avoided remagnetization since being deposited in quartz-rich conglomerates at 2.65–3.05 Ga. To address this issue, we have conducted paleomagnetic conglomerate, baked contact, and fold tests in combination with U–Pb geochronology to establish the timing of the metamorphic and alteration events and the peak temperatures experienced by the zircon host rocks. These tests include the first conglomerate test directly on the Hadean-zircon bearing conglomerate at Erawandoo Hill. Although we observed little evidence for remagnetization by recent lightning strikes, we found that the Hadean zircon-bearing rocks and surrounding region have been pervasively remagnetized, with the final major overprinting likely due to thermal and/or aqueous effects from the emplacement of the Warakurna large igneous province at ~1070 million years ago (Ma). Although localized regions of the Jack Hills might have escaped complete remagnetization, there currently is no robust evidence for pre-depositional (>3.0 Ga) magnetization in the Jack Hills detrital zircons.

1. The early geodynamo and the Jack Hills

The oldest known unmetamorphosed rocks indicate the existence of an active dynamo magnetic field with intensity 50–70% of the present day at 3.450 Ga (Biggin et al., 2011; Tarduno et al., 2010). Due to the lack of older low metamorphic grade rocks, the existence and intensity of the geodynamo during the first ~1 billion years of Earth history—the Hadean eon (>4.0 Ga) and subsequent Eoarchean era (3.6–4.0 Ga)—remain unknown. The early history of the field has important implications for planetary thermal evolution, the physics of dynamo generation, and the oxidation state of the atmosphere (Gomi et al., 2013; Gubbins et al., 2004; Lammer et al., 2008; Nimmo et al., 2004; Tarduno et al., 2014; Ziegler and Stegman, 2013).

The only materials of which we are aware that could possibly retain paleomagnetic records substantially predating 3.5 Ga are detrital zircon crystals found in upper greenschist facies metacon-

* Corresponding author at: Department of Earth, Atmospheric, and Planetary Sciences, Massachusetts Institute of Technology, 77 Massachusetts Avenue, Cambridge, MA 02139, USA. Tel.: +1 617 324 0224; fax: +1 617 258 7401.
E-mail address: bpweiss@mit.edu (B.P. Weiss).

http://dx.doi.org/10.1016/j.epsl.2015.07.067
0012-821X/

glomerates from Erawandoo Hill in the Jack Hills of Western Australia (Holden et al., 2009). With U–Pb crystallization ages ranging from 3.05–4.38 Ga, these zircons are the oldest known Earthly materials. Ferromagnetic inclusions in these zircons have the potential to yield the oldest known records of the geomagnetic field.

The pebble metaconglomerates containing >4 Ga old zircons were deposited at 2.65–3.05 Ga (Rasmussen et al., 2010) and have been subsequently metamorphosed and heavily weathered (Spaggiari, 2007; Spaggiari et al., 2007). A key difficulty with establishing the age of the zircons' magnetization is that these post-depositional processes as well as analogous processes occurring after the zircons formed but prior to deposition in the final 2.65–3.05 metaconglomerate, could have completely remagnetized their inclusions without disturbing the zircons' U–Pb systematics (Mezger and Krogstad, 1997). Laboratory diffusion experiments indicate that a 1 billion year-thermal event at ∼750 °C, which exceeds the Curie points of common ferromagnetic minerals (≤675 °C), will produce just 1% Pb loss from a 100 μm radius non-metamict zircon (Cherniak and Watson, 2000). Therefore, a zircon's magnetization could be far younger than its crystallization age or even disturbance ages inferred from U–Pb discordance. Furthermore, even if could be established that the zircons have not been thermally remagnetized, they still might not retain an ancient magnetization if their ferromagnetic inclusions are secondary (Rasmussen et al., 2011).

A first step toward constraining the age of magnetization in the zircon grains is to establish whether their host conglomerates have been remagnetized since their deposition at 2.65–3.05 Ga. If the rocks have been thermally remagnetized to temperatures exceeding the Curie point of ferromagnetic inclusions in the zircons, this would require that the inclusions themselves were also completely remagnetized by the same event. Alternatively, if the host rocks have been primarily aqueously rather than thermally remagnetized, ancient magnetization might still be retained within primary ferromagnetic inclusions armored against penetrative fluid flow by the surrounding host zircon. Nevertheless, even this favorable case would still leave unknown whether the zircons were remagnetized following their crystallization but before deposition.

The most direct methods for establishing whether rocks retain ancient magnetization are paleomagnetic field tests (Graham, 1949). The basis of the fold test (McElhinny, 1964) is that magnetization that predates (postdates) folding will be less (more) directionally scattered in bedding-corrected coordinates. Similarly, in the baked contact test (Buchan, 2007), country rocks located outside the remagnetization aureole of a younger igneous intrusion and that have magnetization predating (postdating) the intrusion will be magnetized in a different direction from (similar direction to) that of the intrusion. In the conglomerate test, magnetization in clasts of a conglomerate that predates (postdates) deposition of the conglomerates will be collectively randomly (non-randomly) oriented (Watson, 1956). A robust conglomerate test will also demonstrate that the magnetization within individual clasts is consistently oriented in order to exclude the possibility that random clast magnetization directions resulted from fine-scale heterogeneous remagnetization of the conglomerate after deposition.

Recently, Tarduno and Cottrell (2013) reported a paleomagnetic conglomerate test on a quartz-cobble metaconglomerate from the Jack Hills. They identified a high-temperature magnetization component in 27 cobbles that thermally demagnetized from ∼540 °C and 580 °C and was randomly oriented to >95% confidence. They proposed that this positive conglomerate test indicates that the host rocks had not been thermally remagnetized to >540 °C since their deposition. However, this conglomerate test has several limitations, the most important of which are:

(i) The test was conducted 0.6 km from Erawandoo Hill, with the intervening stratigraphy obscured by cover and containing bedding-parallel faults and shear zones (Spaggiari, 2007; Spaggiari et al., 2007). Therefore, the thermal history of the cobbles might differ greatly from that of the >4.0 Ga zircon-bearing Erawandoo Hill conglomerate.
(ii) The abundance of zircons with ∼1700 Ma ages [with one grain as young as 1220 Ma (Grange et al., 2010)] in similar, nearby cobbles means that the conglomerate test may only constrain remagnetization events following as much as 1400 million years after the deposition of the Erawandoo Hill Hadean-zircon bearing conglomerate and after many of the major metamorphic events known to have affected the region.
(iii) For most samples, no overprinting magnetization was identified with a direction unambiguously corresponding to known metamorphic events as indicated by Australia's polar wander path. Such overprint are expected if the cobbles are as old as the 2.65–3.0 Ga Erawandoo Hill conglomerate and have the capability of retaining stable magnetization.

More importantly, this single conglomerate test also leaves the many other rich opportunities for constraining the zircon's magnetization age—fold tests, baked contact tests, and conglomerate tests on other lithologies—unexplored. With this motivation, we conducted two trips to the Jack Hills in 2001 and 2012 to acquire samples for paleomagnetic conglomerate, baked contact, and fold tests and geochronometry that address these limitations. Our goal was to establish the intensity and timing of metamorphic and alteration events to constrain the remagnetization processes experienced by the zircons' host rocks directly at Erawandoo Hill and the surrounding region. Here we report the results of paleomagnetic and radioisotopic analyses of these samples and their implications for the preservation of ancient paleomagnetic records in the Jack Hills zircons.

2. Geology of the Jack Hills

The host rocks of the ancient detrital zircons in the Jack Hills are part of an apparently ∼2 km thick sedimentary succession in fault contact with the surrounding granites and granitic gneisses of the Archean Narryer Terrane (Maas et al., 1992; Spaggiari, 2007; Wilde, 2010) (Fig. 1). The supracrustal rocks are steeply dipping, recumbently folded and thought to pinch out at depth in contact with underlying granite. There are four main sedimentary associations: (1) Archean chert and banded iron formation along the northern and southern margins of the belt, (2) Archean pelitic schists, (3) mature Archean clastic sandstones, quartzites, and conglomerates that include the 2.65–3.05 Ga Hadean detrital zircon host rocks, and (4) Proterozoic quartz-rich rocks (Eriksson and Wilde, 2010; Spaggiari et al., 2007; Wilde and Pidgeon, 1990). The contacts between and within these four associations are often shear zones and/or are obscured by cover. The Hadean detrital zircons have been found almost exclusively within ∼1 km of Erawandoo Hill, mainly in a metaconglomerate containing metamorphically elongated and flattened, cm-sized quartzitic pebbles set in a sandy matrix (Spaggiari, 2007; Spaggiari et al., 2007).

Because the 2.65–3.05 Ga depositional age of the Hadean zircon-bearing sediments postdates the surrounding ∼3.10–3.73 Ga gneisses and porphyritic granitoid rocks (Pidgeon and Wilde, 1998; Spaggiari et al., 2008), the detrital zircon host rocks largely avoided high-grade metamorphism associated with these intrusions. The zircon host rocks nevertheless experienced multiple episodes of thermal metamorphism and aqueous alteration. In particular, quartz–biotite–chloritoid assemblages in siliciclastic rocks indicate upper greenschist facies metamorphism, while grunerite in surrounding banded iron formation and calcic plagioclase–hornblende

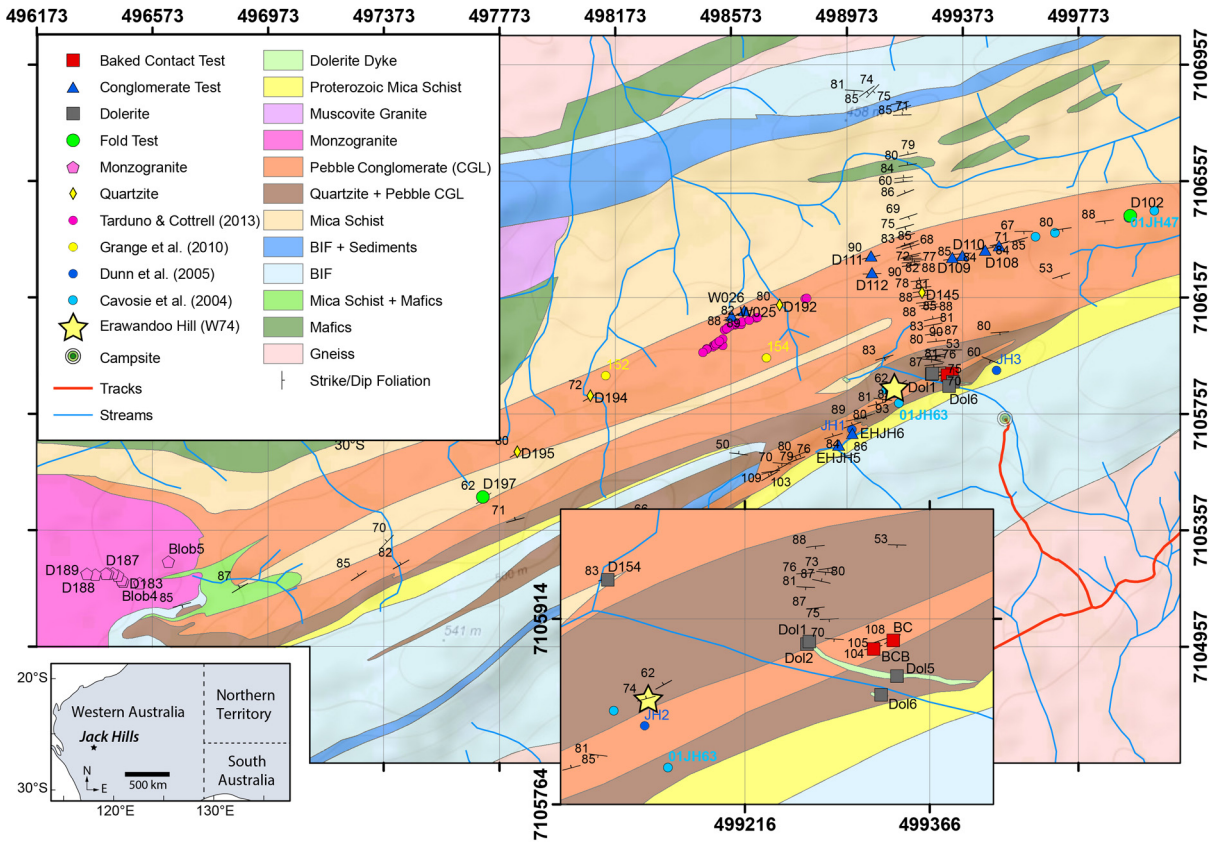

Fig. 1. Generalized geological map of the central-west Jack Hills after Spaggiari (2007). Inset at bottom left shows regional location in Western Australia. (A) Overview of sampling area. Lithologies are denoted by light shaded colors. Our baked contact, fold, and conglomerate test sites are noted. Yellow star denotes discovery site of >4 Ga zircons (Erawandoo Hill, also known as W74). Locations of Proterozoic detrital zircons sampled by Cavosie et al. (2004), Dunn et al. (2005), and Grange et al. (2010) are denoted by small light blue, dark blue and yellow circles. Sampling localities for individual cobbles sampled by Tarduno and Cottrell (2013) are shown by small magenta circles. All geological contacts are estimated. Stratigraphic up direction is frequently ambiguous within the quartzites and conglomerates, but is usually toward the southeast. Magnetic declination was set to zero degrees; the estimated local declination was ~0.4°. Projection is with the Universal Transverse Mercator grid in the World Geodetic System 1984 standard. Spacing between contour lines (grey) is 50 m.

assemblages in mafic schists indicate at least localized amphibolite facies metamorphism (Spaggiari, 2007; Spaggiari et al., 2007; Wilde and Pidgeon, 1990). Monazite–xenotime and Ti-in-quartz thermometry suggest that the Erawandoo Hill conglomerates reached ~346–487 °C (Rasmussen et al., 2010). As described in the Supplemental Materials (SM), there were at least four major thermal and deformational events that likely affected the zircon host rocks: (i) thermal metamorphism at 2654 Ma due to monzogranite intrusions linked to the assembly of the Yilgarn craton; (ii) thermal disturbances associated with the 1960–2005 Ma Glenburgh orogeny; (iii) thermal disturbances and large-scale shearing associated with the Capricorn orogeny at 1780–1830 Ma; and (iv) emplacement of the Marnda Moorn and Warakurna large igneous provinces (LIPs) at ~1210 and ~1070 Ma, respectively.

We conducted three baked contact tests associated with a dolerite dyke intruding quartzitic rocks and pebble conglomerate, two fold tests associated with folds within quartzitic rocks, three conglomerate tests associated with the Erawandoo Hill Hadean zircon-bearing pebble conglomerates, and three conglomerate tests associated with cobble conglomerates of similar lithology and in close proximity to those studied by Tarduno and Cottrell (2013). We also sampled lithologies distributed throughout the central Jack Hills, including a 2654 Ma monzogranite intruding the supracrustal rocks, to establish the larger spatial scale of remagnetization from both the dolerite and the monzogranite intrusions. Our sample localities are shown in Fig. 1.

3. Rock magnetism and petrography

3.1. Overview

We characterized the ferromagnetic mineralogy and magnetic properties of the Jack Hills rocks to establish their fidelity for recording remagnetization events and to constrain their alteration history. We conducted rock magnetic analyses of chips and powders and optical and electron microscopy of polished 30 μm thin sections from samples of the major lithologies subjected to paleomagnetic analyses.

3.2. Thermal demagnetization of three-axis isothermal remanent magnetization (IRM)

To determine peak unblocking temperature as a function of coercivity, twenty samples were each given a three-component IRM and progressively thermally demagnetized. The composite IRM was produced by exposure to 4 T along the sample z-axis followed by 0.36 T and then 0.12 T along the x- and y-axes, respectively. Given the peak coercivities for common ferromagnetic minerals (Dunlop and Özdemir, 1997), z-axis magnetization should be carried by hematite (Néel temperature ~675 °C), goethite (Néel temperature of ~50–120 °C), and pyrrhotite (Néel temperature ~320 °C), x-axis magnetization should dominantly reflect pyrrhotite and magnetite, and y-axis magnetization should reflect pyrrhotite, magnetite and titanomagnetite (Dekkers, 1989; Lowrie, 1990; Özdemir and Dunlop, 1996). Moment measurements were acquired with a 2G En-

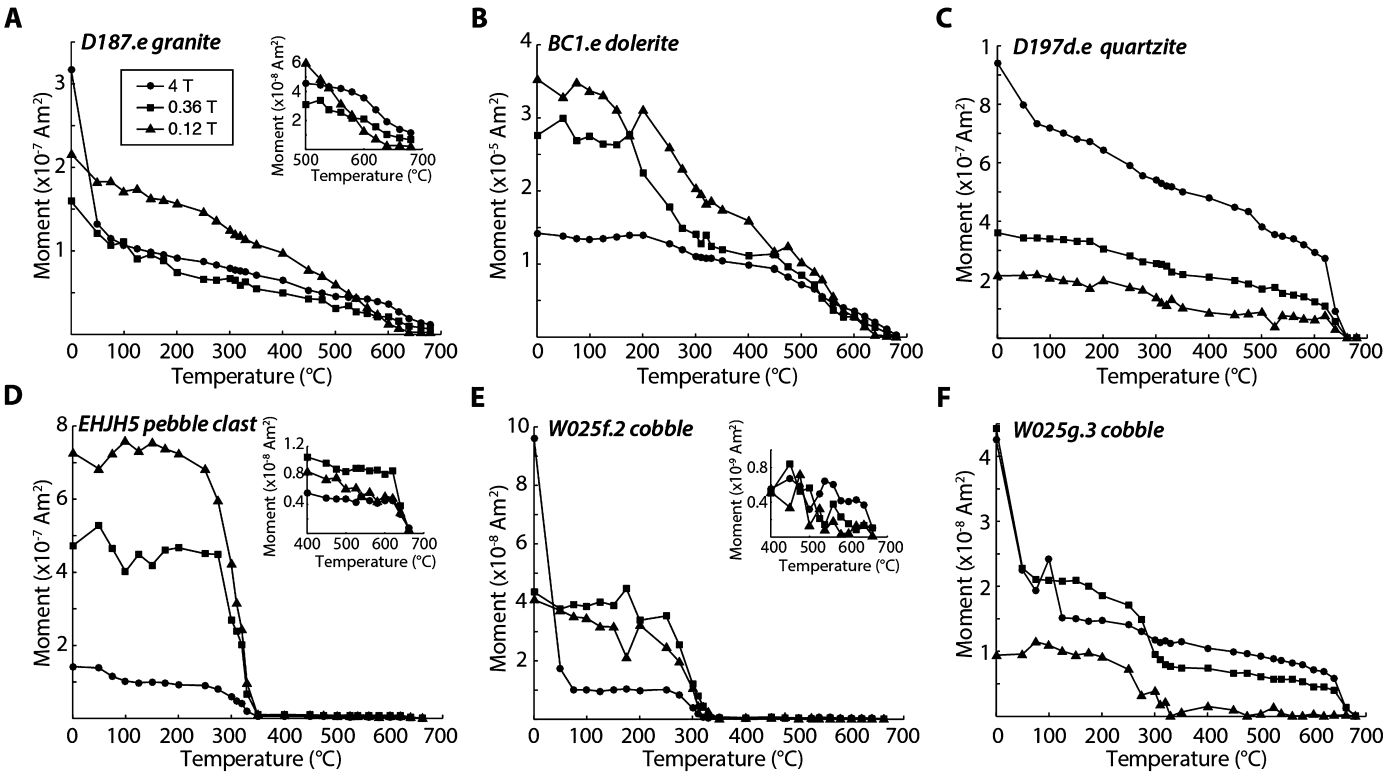

Fig. 2. Selected examples of thermal demagnetization of a three-component IRM produced by magnetizing the sample in a 4 T field along the *z*-axis, followed by 0.36 T along the *x*-axis, and 0.12 T along the *y*-axis. Each plot contains curves showing the corresponding *z*- (circles), *y*- (squares), and *x*- (triangles) magnetization components. (A) Monzogranite sample D187.e. (B) Dolerite sample BC1.e. (C) Quartzitic fold test sample D197d.e. (D) Clast from Erawandoo Hill pebble conglomerate EHJH5c. (E) Clast from cobble conglomerate W025f.2. (F) Clast from cobble conglomerate W025g.3. See Fig. S2 for more examples of thermal demagnetization of three-axis IRM.

terprises Superconducting Rock Magnetometer (SRM) 755 in the UC Berkeley Paleomagnetism Laboratory.

The results (Figs. 2 and S2) show that the monzogranite contains predominantly magnetite and goethite with some of hematite, while the dolerite contains mostly magnetite with a small quantity of pyrrhotite and hematite. Quartzitic rocks from the fold test sites contain hematite and goethite (at site D197) and pyrrhotite, goethite, and lesser magnetite (at site D102). Erawandoo Hill conglomerate pebble clasts contain almost exclusively pyrrhotite, the Erawandoo matrix contains additional hematite, and cobble clasts from the cobble conglomerate contain dominantly pyrrhotite with lesser hematite and goethite and minor quantities of magnetite.

3.3. Other rock magnetic experiments

We measured temperature-dependent susceptibility of cobbles from ~25–700 °C in both air and Ar (Fig. 3). When heating in air, most cobbles heated in air showed weak susceptibility signals (Fig. 3C, F and S1B), with a single exception that exhibited a susceptibility peak indicating the generation magnetite (Fig. 3A), possibly from sulfide alteration. Heating in Ar above ~400 °C led to the generation magnetite (Figs. 3B, D, E, G, S1D) presumably due to reduction of hematite or other oxidized phases. There is no evidence for pyrrhotite in any of our susceptibility data.

We also conducted low temperature cycling experiments on both fresh cobble samples as well as those previously subjected to the high temperature susceptibility measurements. The loss of remanence across the low temperature Besnus (~35 K) and Verwey (~120 K) transitions (Fig. 3E and SM) indicates the presence of pyrrhotite along with some magnetite. These data also confirm that magnetite was produced during the high-temperature susceptibility measurements and also show that pyrrhotite was destroyed during the susceptibility measurements (see Fig. 3E and F and SM).

Our room temperature hysteresis and back field remanence measurements (Fig. S3 and SM text) show that the mean ferromagnetic grain size for all analyzed samples except for the monzogranites is pseudo single domain, with the monzogranites likely containing a mixture of multidomain and single domain magnetite and hematite plus goethite, respectively.

3.4. Optical and electron microscopy

We conducted optical microscopy, backscattered electron microscopy (BSEM), electron dispersive spectroscopy, and wavelength dispersive spectroscopy (WDS) to constrain the composition, grain size, textural relationship, and origin of the ferromagnetic minerals. We found that the Erawandoo Hill conglomerate matrix contains abundant secondary hematite and the Erawandoo conglomerate and cobble conglomerate clasts contain predominantly iron sulfides and relatively few iron oxide grains (Fig. 4). WDS demonstrates that these sulfides are ferromagnetic monoclinic pyrrhotite and the nonmagnetic minerals pyrite, pentlandite and chalcopyrite (Fig. 4). Iron oxides in the Erawandoo Hill conglomerate are mainly in the form of FeOOH (including goethite) and hematite, whereas the cobble conglomerates contained hematite and magnetite grains.

3.5. Summary of ferromagnetic mineralogy

Collectively, our data show that the ferromagnetic minerals in the monzogranite and dolerite are dominantly iron oxides (mainly magnetite and goethite, with a secondary contribution from hematite), quartz clasts in the pebble and cobble conglomerates contain dominantly pyrrhotite with a secondary contribution from goethite and hematite and minor magnetite, and the quartzites and conglomerate matrices contain dominantly

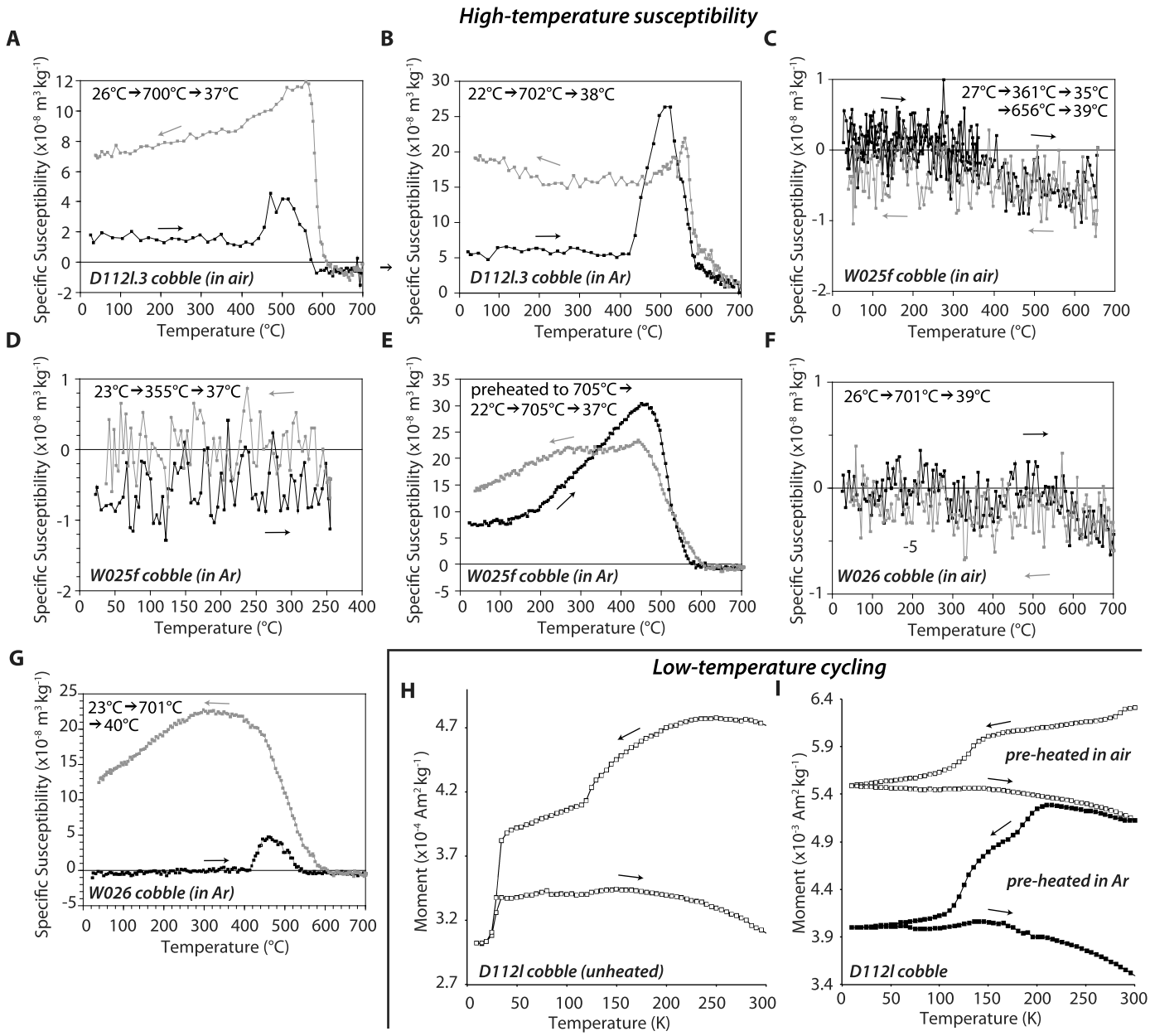

Fig. 3. High temperature susceptibility (A–G) and low temperature cycling of room temperature saturation IRM measurements (H, I) on Jack Hills cobbles. (A) D112l.3 cycled in air up to 702 °C. (B) D112l.3 cycled in Ar cycled up to 702 °C. (C) W025f cycled in air first to 361 °C and then to 656 °C. (D) W025f cycled in Ar up to 355 °C. (E) W025f cycled in Ar up to 705 °C. Prior to these measurements, sample had been previously heated in Ar up to 705 °C (see Fig. S1D). (F) W026 cycled in air up to 701 °C. (G) W026 cycled in Ar up to 701 °C. (H) D112l unheated. (I) D112l previously subjected to temperature-dependent susceptibility analyses in air and Ar [see (B)]. See Fig. S1 for more examples of high-temperature susceptibility data.

hematite, goethite, and pyrrhotite. Our observations of the cobble conglomerate mineralogy differ from those of Tarduno and Cottrell (2013), who inferred from high-temperature susceptibility data that their cobbles contain dominantly magnetite. Our data demonstrate that such measurements can obscure the presence of pyrrhotite and overemphasize the presence of magnetite due to destruction of sulfides and the production of iron oxides during the heating experiment.

4. Paleomagnetism and geochronology

4.1. Overview

In the field, we sampled oriented blocks using magnetic and sun compasses. Later at MIT, we drilled 25 mm-diameter cores (for all samples but most cobble conglomerates and the Erawandoo Hill pebble conglomerates), 12-mm diameter cores (from most of the cobble conglomerates), and microsampled mm-scale chips using a low-speed saw and hand drill (from the Erawandoo Hill pebble conglomerate). We named our samples after the field site at which they were acquired, followed by a letter and/or number for sites yielding multiple samples. To assess reproducibility, we often analyzed multiple subsamples from each of these samples; the names of these subsamples have a suffix consisting of a period followed by the subsample number.

We subjected most samples to stepwise alternating field (AF) demagnetization up to 10 mT. We then thermally demagnetized all subsamples up to peak temperatures ranging up to 680 °C and measured their moments with a 2G Enterprises SRM 755 equipped with an automatic sample handling system (Kirschvink et al., 2008) in the MIT Paleomagnetism Laboratory (demagneti-

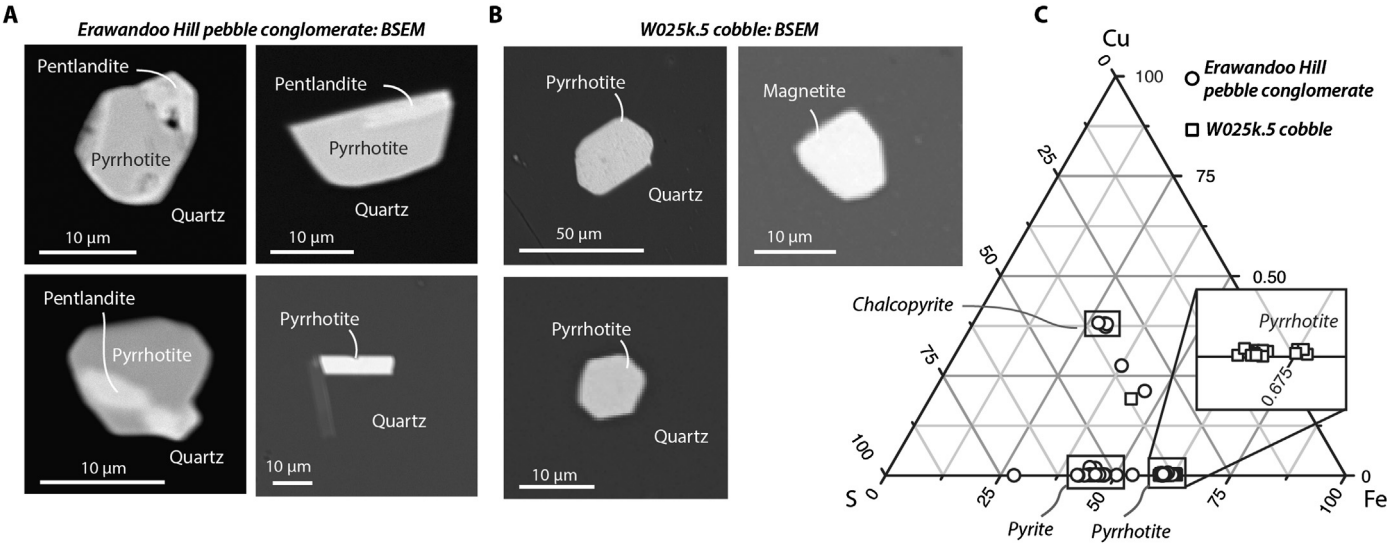

Fig. 4. Electron microscopy of Jack Hills conglomerate clasts. (A) BSEM images of iron sulfides in quartz clasts from the Erawandoo Hill pebble conglomerate. (B) BSEM images of pyrrhotite and magnetite in quartz cobble sample W025k.5. (C) WDS compositional analyses of sulfides in Erawandoo pebble conglomerate and W025k cobble. The observed ratios of Fe, S, and Cu indicate the presence of monoclinic pyrrhotite, pyrite, and chalcopyrite. Inset shows magnification around pyrrhotite composition; for clarity, measurements shown from only W025k.5.

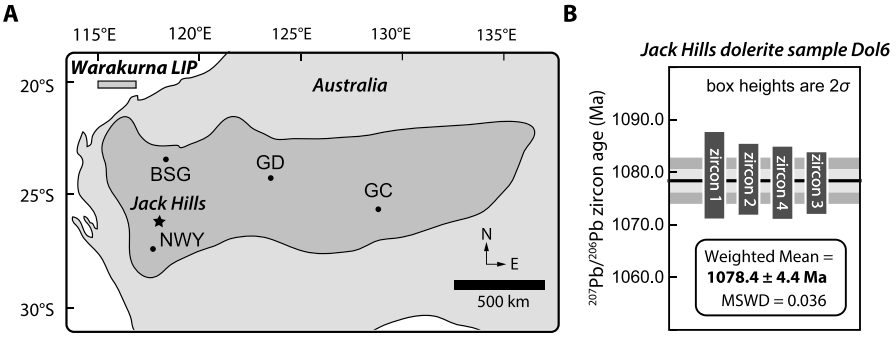

Fig. 5. (A) Geographic extent of the Warakurna LIP in west Australia, including its major mafic sill and dyke intrusions and their published sensitive high-resolution ion microprobe (SHRIMP) U–Pb dates (2σ uncertainties) from Wingate et al. (2004). BSG = Western Bangemall Supergroup sills: 1071 ± 8 Ma, 1067 ± 14 Ma and 1068 ± 22 Ma; GC = Giles Complex: 1073 ± 5 Ma and 1058 ± 14 Ma; GD = Glenayle Dolerite: 1063 ± 21 Ma and 1068 ± 20 Ma; NWY = Northwest Yilgarn dykes: 1075± 10 Ma. Star denotes location of Jack Hills. See Wingate et al. (2004) for U–Pb radioisotopic age uncertainties, methods, and references. (B) Date distribution plot for the analyzed zircons from dolerite dyke adjacent to Erawandoo Hill in the Jack Hills. Vertical axis is measured ^{207}Pb/^{206}Pb date; bar heights represent 2σ analytical uncertainty of individual analyses. Shaded horizontal bands and their width signify uncertainty in the weighted mean date at 1σ and 2σ levels. MSWD is mean square of weighted deviates. See SM for detailed U–Pb data and interpretation.

zation data are provided in the SM). Natural remanent magnetization (NRM) components were estimated using principal component analysis (Kirschvink, 1980) (Table S2).

AF demagnetization sometimes isolated low coercivity (LC) components. Subsequent thermal demagnetization often isolated additional components at low temperatures (LT), sometimes followed by origin-trending high temperature (HT) components. Occasionally, samples contained one or two additional medium temperature (MT) components, while many samples (particularly the cobbles) contained no coherent origin-trending HT component. Unless noted otherwise, magnetization directions are reported in geographic (i.e., in situ) coordinates rather than bedding-corrected coordinates. See SM for more details about how components were named and identified.

We note that only six samples (monzogranite sample D189, quartzite samples BC5 and BCB9, and three cobbles from sites W025 and W026) showed compelling evidence for lightning remagnetization, as indicated by anomalously high magnetizations (typically two orders of magnitude greater than surrounding rocks of similar lithology), single-component linear demagnetization trends, and anomalous magnetization directions. One of these parent sites (W025) also showed evidence for a lightning strike anomaly as indicated by deflection of a magnetic compass needle.

4.2. Dolerite baked contact tests

A west–northwest trending dolerite dyke crosscuts interbedded conglomerate, quartzite, and siltstone about 200 m northeast of Erawandoo Hill (Fig. 1 inset). The exposed portion of the dyke is ~250 m long and has a half-width, r_{dyke}, of ~5 m. It exhibits no evidence of deformation and cuts across fold structures and Proterozoic sedimentary rocks. The dyke previously has been correlated with the ~1070 Ma Warakurna LIP (Spaggiari, 2007; Spaggiari et al., 2007), an extensive series of intrusions, dykes, and volcanic rocks in central and Western Australia (Wingate et al., 2004) (Fig. 5A). Our U–Pb isotope dilution thermal ionization mass spectrometry zircon weighted mean ^{207}Pb/^{206}Pb date of 1078.4± 3.4/4.4/6.6 Ma from the dolerite (Fig. 5B and SM) confirms the dyke's association with the Warakurna LIP.

We conducted baked contact tests at three locations (sites BC, BCB, and D154) distributed along the strike of this and an adjacent dyke to establish the remagnetization history since 1078 Ma (Figs. 1 and 6A). At each site, samples were acquired of the

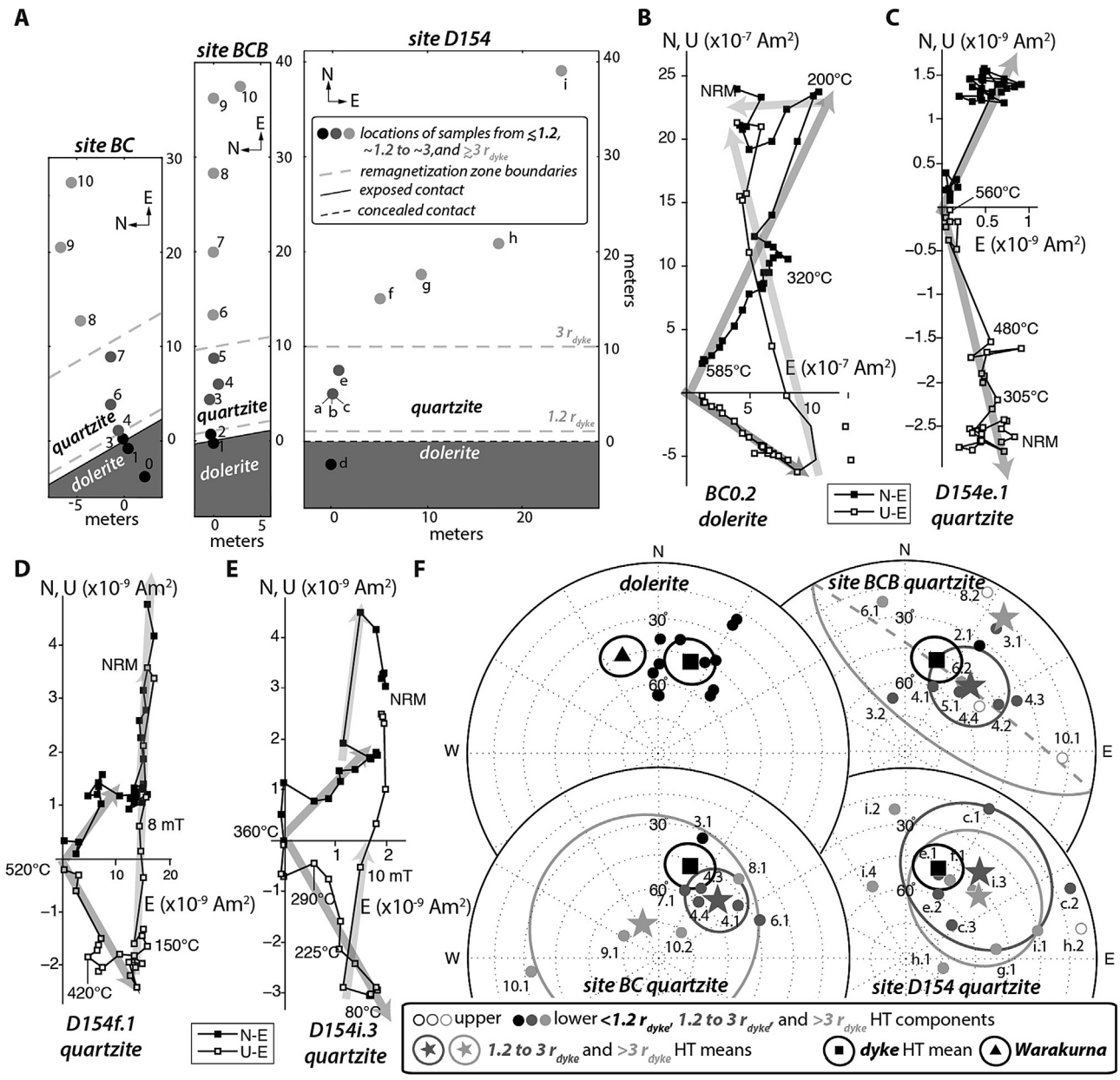

Fig. 6. Dolerite baked contact tests at sites BC, BCB, and D154. (A) Simplified maps showing locations of dolerite and quartzitic country rock samples (circles) at each site. The shade of each point corresponds to distance of sample from center of dyke and dashed grey lines denote approximate boundaries of thermal remagnetization zones assuming simple thermal diffusion (see text). Solid and dashed black lines denote observed and concealed contact, respectively, between dolerite and quartzite. (B–E) Two-dimensional projection of the endpoint of the NRM vector during AF and thermal demagnetization in geographic coordinates for dolerite sample BC0.2 (B) and quartzitic samples D154e.1 (C), and D154f.1 (D), and D154i.3 (E). Closed and open symbols represent end points of magnetization projected onto north–east (N–E) and up–east (U–E) planes, respectively. Peak AC fields and temperatures for selected AF and thermal demagnetization steps are labeled. Also shown are LT (lighter arrows) and HT (dark arrows) components. (F) Equal area stereonet showing directions of HT components from the dolerite at all three sites (top left) and quartzitic rocks from sites BCB (upper right), site BC (lower left), and site D154 (lower right). Open and closed symbols represent upper and lower hemispheres. Also shown are Fisher HT mean directions and associated 95% confidence ellipse from dolerite (squares) and country rock samples from outer two thermal remagnetization zones (dark and light gray stars) at sites BCB, BC, and D154. Triangle and associated ellipse denotes local paleomagnetic field direction and 95% confidence interval for mean pole for Bangemall Supergroup sills (part of Warakurna LIP) (Wingate et al., 2002).

dyke and from quartzitic country rock at progressively larger distances from the dyke. Thermal diffusion calculations indicate that a basaltic sheet dyke should heat intruded silicate country rock to ~530–580 °C, ~350 °C, and ~170 °C at distances of 1.2, 2, and 4 dyke radii from the dyke center assuming purely conductive heat transport [see Table 2 of Jaeger (1964)]. Therefore, given the peak unblocking temperatures observed for the country rocks (see below), if conductive heating by the dyke has been the only process that has remagnetized the country rock, we expect that samples at distances of $<\sim 1.2r_{dyke}$, between ~1.2 and $\sim 3r_{dyke}$, and $>\sim 3r_{dyke}$ should lie in the fully remagnetized, partially remagnetized, and weakly baked zones.

We found that individual unweathered dyke samples from the three sites typically contained two but sometimes up to five NRM components (Fig. 6B–F). LT components are directionally clustered with a mean direction close to the present geomagnetic field (Figs. 6 and S6A). Nearly all samples contained a consistently-oriented, origin-trending HT component that unblocked between 100–440 °C and 530–580 °C, sometimes with a small remanence (almost always <5% of NRM) persisting above 580 °C. The peak

unblocking temperature of the HT component along with our rock magnetic data (Section 3) indicate it is carried primarily by magnetite, with a small contribution from hematite. Because the HT directions carried by both minerals are similar, it is likely that the hematite was produced by oxidation of magnetite during or soon after emplacement. A small number of samples (i.e., BC0.1, Dol5.1 and Dol5.2) exhibited a weak reversed component above 540 °C that may be a self-reversal associated with martite [e.g., Swanson-Hysell et al. (2011)]. The dyke mean HT direction (declination 19.3°, inclination 47.5°, $\alpha_{95} = 10.1°$, and estimated Fisher precision parameter $k = 17.9$) has a virtual geomagnetic pole (VGP) located at latitude $\theta = 32.2°$N and longitude $\varphi = 137°$E (95% confidence ellipse with semiaxes of $dp = 8.5°$ and $dm = 13.1°$). Assuming a typical rock thermal diffusivity of $D = 10^{-6}$m^2 s^{-1}, the dyke should have required a time $t \approx r_{dyke}^2/D \approx 1$ yr to diffusively cool from the magnetite Curie point to ambient temperatures, meaning that its VGP should not average typical secular variation. Allowing for this, the pole is broadly similar to that of Warakurna LIP rocks (e.g., the Bangemall basin dolerite sills: $\theta = 33.8°$N and longitude $\varphi = 95.0°$E, 95% confidence interval $A_{95} = 8.3°$, modified quality criterion AV value = 6 out of 6) (Wingate et al., 2004) (Fig. 6F).

Individual country rock samples near the dolerite at the three sites contained between one and three NRM components. Although the demagnetization trends are noisy for many samples, multiple subsamples from individual cores usually yield similar components (e.g., cores BCB4 and D154i). Most samples contained a LT component removed by 80–440 °C depending on the sample. The LT components collectively are scattered but have a mean direction within error of the present geomagnetic field, suggesting a recent origin (Fig. S6B). Most samples contained an origin-trending HT component with maximum unblocking temperatures ranging from 225 to 580 °C (and usually >500 °C). The combined mean HT directions for each of the fully baked, partially baked and weakly baked zones for the three sites (Table S2) are essentially indistinguishable from the dolerite HT mean (Fig. 6F), indicating failed baked contact tests. The country rock, even at the maximum sampling distance of $7.8r_{dyke}$, is magnetized in the direction of the dyke. Because this is far beyond the expected conductive thermal remagnetization zone, it suggests that regional-scale thermal and/or chemical remagnetization affected the Erawandoo Hill as a result of the Warakurna LIP.

4.3. Monzogranite and quartzitic country rock

Further evidence for regional-scale remagnetization is provided by our analyses of monzogranite and country rock from 14 sites distal to the dyke. In particular, we analyzed the 2654 ± 7 Ma monzogranite intruding supracrustral rocks ~3 km to the west-southwest from Erawandoo Hill ("The Blob") (Wilde and Pidgeon, 1990) (D182–D189, Blob4, and Blob5) and quartzites and quartz pebble conglomerates (sites D192, D194, D195, and D196) located 0.8 to 2 km to the west of Erawandoo Hill (Fig. 1). Thermal diffusion calculations (Section 4.2) indicate that sites D194, D195, D196, along with fold site D197 (see Section 4.4), should be within the partial to full thermal remagnetization zone of the monzogranite Blob and therefore constitute another large-scale baked contact test for remagnetization since 2654 Ma.

We found that most monzogranite samples contained an LT component removed by 80–290 °C that is indistinguishable from that of the present geomagnetic field (Figs. 7 and S6C). This common direction and the abundance of goethite in some of these samples (Section 3) indicate that the LT component likely was produced by recent oxidative weathering. Nearly all samples also contained an HT component that unblocked from the end of the LT component up to a maximum temperature of nearly 580 °C (Fig. 7). The mean HT direction is indistinguishable from the Warakurna LIP local paleofield direction (Section 4.2).

We found that most quartzitic rocks also carried LT components that thermally demagnetized up to 80–360 °C. Although collectively scattered, their mean is within error of the present geomagnetic field, consistent with a recent origin (Fig. S6). Sites D192, D194, D195, and D197 also contain an HT component (removed from the end of the LT component usually up to a maximum temperature of 290 to 360 °C, but reaching 520 °C for sample D194c) with a mean direction near the Warakurna LIP local paleofield direction (Figs. 7 and S6D).

4.4. Fold tests

We identified two meter-scale folds in metamorphosed quartz pebble conglomerates 0.7 km northeast (D102) and 2.0 km west (D197) of Erawandoo Hill (Figs. 1 and 8). At site D102, there is a southeast verging fault propagation fold with 10 cm scale parasitic folding superimposed on the meter-scale hinge zone. The fault bend is not deformed, but the entire structure is rotated with the bedding (074/82) such that the fold hinge line is near-vertical. At site D197, there is a southeast-verging kink band within beds with strike/dip = 234/62. The steeply-plunging fold axes within strongly sheared beds suggest that the meter-scale folding is older than the map-scale regional tilting of the meta conglomerates and sandstones. At a minimum, the cross-cutting relationship requires the meter-scale folding to be older than intrusion of the dolerite dyke. At both sites, oriented samples were collected from a variety of orientations around major and parasitic fold hinges.

We found that most samples from site D102 have scattered LT components that unblocked up to ~200–275 °C with a mean direction close to the present geomagnetic field (Figs. 8 and S6E). Given this common direction and the abundance of goethite in these samples (Section 3), the LT components are likely of recent origin. All samples but D102c also contained an origin-trending HT component blocked up to 325–350 °C. The HT directions are equally scattered in both in situ (i.e., geographic) and bedding-tilt coordinates (ratio of estimated Fisher precision parameters with and without tilt correction $k_{tilt}/k_{geo} = 1.0$). Therefore, the fold test at this site is inconclusive (does not pass at the 95% confidence interval).

We found that site D197 samples exhibited typically weak and scattered LT components that unblocked up to 100–300 °C (Figs. 8 and S6F). All samples contained a dominant MT component that unblocked up to 325–350 °C and many samples also contained a weak HT component that unblocked up to 640 °C (Figs. 8 and S7). The MT components become more scattered after bedding tilt-correction ($k_{tilt}/k_{geo} = 0.46$) and therefore fail the fold test. Furthermore, the MT directions in geographic coordinates are well-clustered and within error of the local mean Warakurna LIP paleofield direction (Section 4.3). The fold test for the HT directions is inconclusive ($k_{tilt}/k_{geo} = 1.4$, such that it does not pass the fold test at the 95% confidence interval); given that the HT mean direction is within error of the present geomagnetic field direction and is carried by hematite [as required by its peak unblocking temperature and supported by our rock magnetic data (Section 3)], it probably originated during recent oxidative weathering.

4.5. Conglomerate tests

4.5.1. Erawandoo Hill pebble conglomerate

We conducted three paleomagnetic conglomerate tests on mm-diameter quartz clasts from three blocks sampled from three sites (EHJH5, EHJH6, and EHJH7) in the Erawandoo Hill Hadean zircon-bearing pebble conglomerate (Fig. 1). A total of 55 oriented clasts and 29 oriented bulk matrix samples were extracted from each

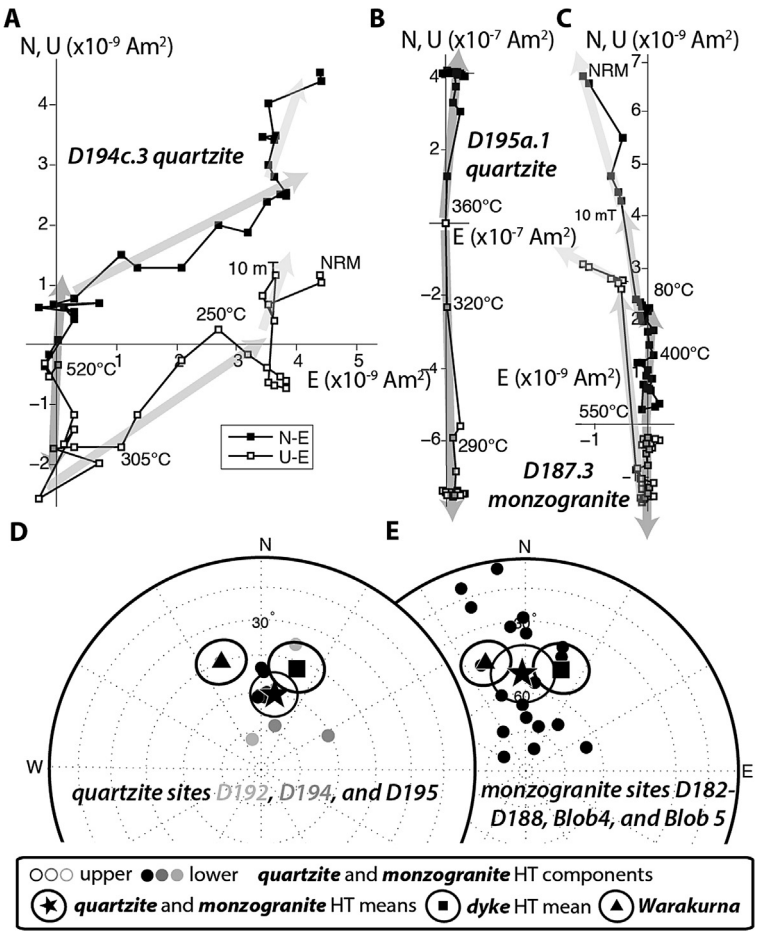

Fig. 7. Paleomagnetism of monzogranite and quartzite. Two-dimensional projection of the endpoint of the NRM vector during AF and thermal demagnetization in geographic coordinates for quartzitic samples D194c.3 (A) and D195a.1 (B) and monzogranite sample D187.3 (C). Closed and open symbols represent end points of magnetization projected onto north–east (N–E) and up–east (U–E) planes, respectively. Temperatures for selected thermal demagnetization steps are labeled. Also shown are LC (lightest arrows), LT (intermediate shaded arrows) and HT (dark arrows) components. (D, E) Equal area stereonet showing directions of HT components from the quartzite sites D192 (light grey), D194 (dark grey), and D195 (black) (D) and monzogranite sites D182–D188, Blob4 and Blob5 (E). Open and closed symbols represent upper and lower hemispheres. Stars, square and triangle with associated ellipses denote monzogranite and quartzite HT means, dolerite HT mean (Fig. 6F), and local paleomagnetic field direction for mean pole for Bangemall Supergroup sills (part of Warakurna LIP) (Wingate et al., 2002) with 95% confidence intervals, respectively.

block using nonmagnetic dental tools and saws. Seven of these clasts were further subdivided into a total of 21 subsamples to test whether the clast magnetization in the clasts is unidirectionally oriented. The samples were mounted on 25 mm diameter nonmagnetic GE 124 quartz disks using nonmagnetic adhesives.

We found that most samples have an LT component that thermally demagnetized by ~150–250 °C (Fig. 9). The LT components in EHJH5 have a mean direction within error of the present local geomagnetic field and therefore likely originated recently (Fig. S6G). Many samples also have an origin-trending HT component that unblocked from the end of the LT component up to between 325–350 °C (and persisting up to at least 500 °C for one sample). Many other samples (particularly from EHJH6) never reached origin-trending trajectories due the acquisition of spurious remanence during demagnetization. The distribution of HT components that were inferred from EHJH6 extends asymmetrically toward the block's mean LT direction, suggesting that the two components are carried by grains with overlapping blocking temperatures. This may also explain why the LT components from EHJH7 differ in direction and are within error of the HT direction for this block (Fig. S6H).

The stable HT components isolated from clast and matrix samples are dominantly unidirectionally oriented within each block. In particular, 30 clasts from EHJH5 and 10 clasts from EHJH6 are nonrandomly magnetized at >99% confidence (resultant vectors $R = 28.2$ and 6.9, respectively), while 2 clasts from EHJH7 are also highly clustered. This result indicates that the characteristic magnetization of all three blocks was acquired after deposition of the conglomerate at 3.0–2.65 Ga. The grand HT mean for the three blocks is indistinguishable from the local Warakurna LIP paleofield direction, suggesting remagnetization by this ~1070 Ma igneous event. Although the mean directions of the three blocks are distinct to >95% confidence from the Warakurna LIP direction, all subsamples from each block are from just several cm of stratigraphy (and so the block means are unlikely to completely average secular variation) and all share the same orientation of their parent block (and so are subject to systematic errors associated with orienting the parent block and deviation of the block's orientation from that of the local mean bedding).

4.5.2. Cobble conglomerate

Conglomerates containing large (0.5–30 cm long) cobbles outcrop ~500 m northwest of Erawandoo Hill (Fig. 1). These cobbles are elongated and metamorphically flattened and composed mainly of quartz, chert and quartzite and are supported in a sandy matrix. We sampled 35 cobbles at 9 sites distributed 1.6 km along strike in the cobble beds (sites D107–D112, D192, W025, and W026), with the latter two sites located within ~37 m of the samples of Tarduno and Cottrell (2013). This yielded enough samples for three separate conglomerate tests: at sites D111, D112, and a

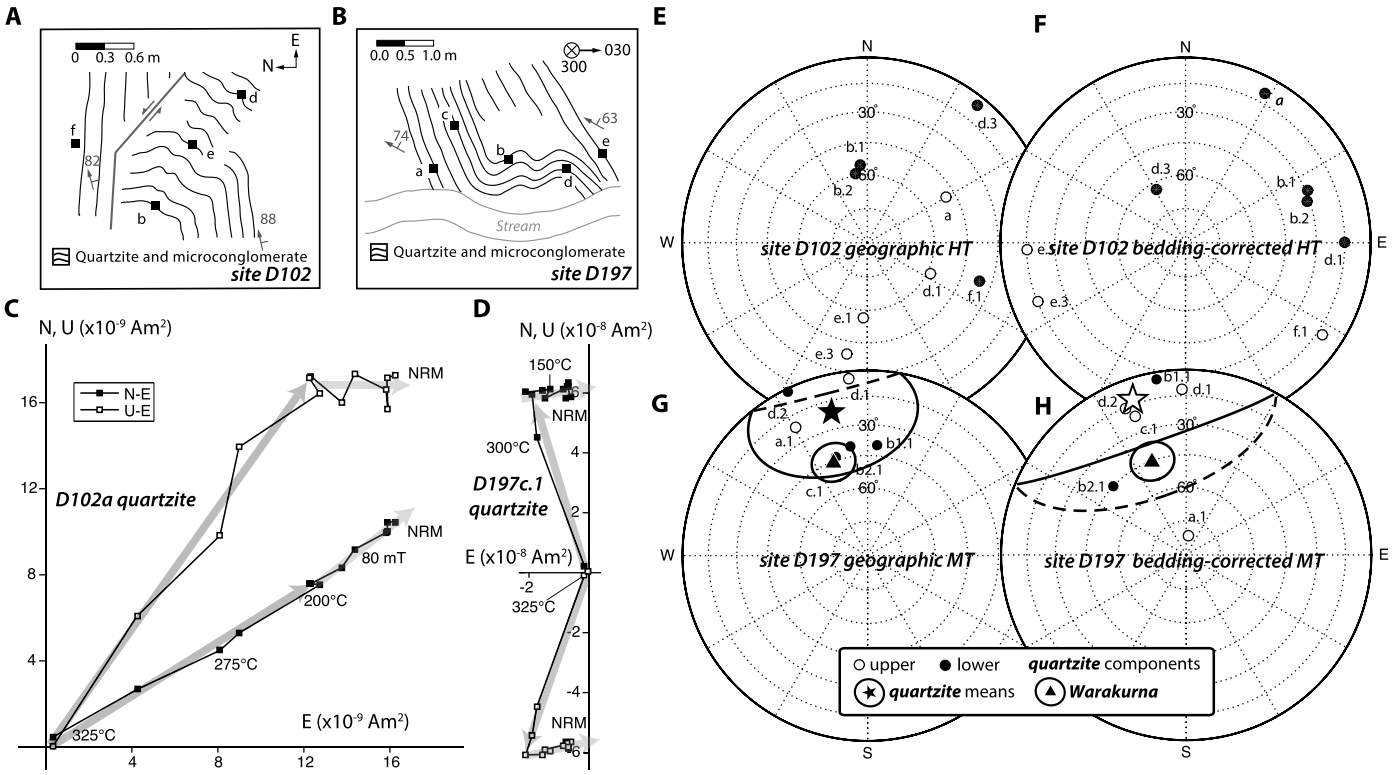

Fig. 8. Fold tests at sites D102 and D197. (A, B) Simplified map of D102 (A) and D197 (B) sites showing sample location (squares), bedding planes (curvy lines), field measurements of bedding strikes (hatched arrows) and dips (numbers), sinistral fault [grey line with grey arrows in (A)] and streambed [light grey lines in (B)]. Scale bars are 0.6 m (A) and 1.0 m (B). Compasses denote geographic north and east (A) and declinations 30° and 300° (B). (C, D) Two-dimensional projection of the endpoint of the NRM vector during AF and thermal demagnetization in geographic coordinates for quartzitic samples D102a.1 (C), and D197c.1 (D). Closed and open symbols represent end points of magnetization projected onto north–east (N–E) and up–east (U–E) planes, respectively. Peak AC fields and temperatures for selected AF and thermal demagnetization steps are labeled. Also shown are LT components (lighter arrows) and HT (for D102a) and MT (for D197c.1) components (dark arrows). (E–H) Equal area stereonet showing directions of HT components from the quartzitic site D102 in geographic (E) and bedding-corrected coordinates (F) and MT components from quartzitic site D197 in geographic (G) and bedding-corrected coordinates (H). Open and closed symbols represent upper and lower hemispheres. Stars and triangle and associated ellipses denote site D197 MT means and local paleomagnetic field direction for mean pole of Bangemall Supergroup sills (part of Warakurna LIP) with 95% confidence intervals (Wingate et al., 2002), respectively.

test combining adjacent sites W025 and W026. At each of these sites, the cobbles were sampled at most <5 m apart to ensure that they have similar depositional ages, metamorphic histories, and have not experienced within-site differential rotation [whereas the samples of Tarduno and Cottrell (2013) were acquired over a ~200 m area]. Our samples generally are from the same lithologic population but are probably not from the very same beds as those sampled by Tarduno and Cottrell (2013). Detrital zircon dates (Grange et al., 2010) show these conglomerates were probably deposited after 1.7 Ga (and perhaps after 1.22 Ga).

At MIT, we drilled 13 mm or 25 mm diameter cores through the centers of each cobble. We then sliced the cores and acquired individual subsamples from near the center of each core and away from any apparent fractures and secondary alteration. For most cobbles, we obtained two subsamples to test for homogeneity of NRM. The samples from the 13 mm cores were mounted on 25 mm diameter nonmagnetic GE 124 quartz disks using double-sided tape. The disk mounts were regularly cleaned and their moments measured after each demagnetization step to ensure that their moments remained no more than 5% of those of the samples.

Unlike other Jack Hills samples analyzed in this study, the majority of cobbles exhibited highly unstable demagnetization behavior (Figs. 10 and S9). In most cases, the little modestly stable demagnetization behavior observed was in the form of LC (removed by <10 mT) and/or LT (unblocked by 100–275 °C) components that are collectively scattered (Figs. 10A and S6J–L). After removal of this component, most cobbles exhibited large directional changes, often without decaying in moment or ever settling to an origin-trending direction. Furthermore, subsamples from these cobbles usually exhibited strikingly nonhomogeneous NRM directions and demagnetization trends (Fig. 10).

As a result, we identified origin-trending HT components from only 22 out of 61 subsamples (15 out of 35 cobbles). Even for these 15 cobbles, we were only able to demonstrate that 7 have homogeneous intra-cobble HT components (Table S2). No such stably magnetized cobbles were identified from sites D111 and D112, while only 4 such cobbles were identified from the combined W025 and W026 site (Fig. S8). However, the significance of even these four samples is highly suspect: three are likely lightning-remagnetized (they have only a single magnetization component, have the strongest NRM intensities among samples at these sites, and a magnetic anomaly was observed near the W025 sampling site from magnetic compass field observations), while the HT component of the fourth is carried by hematite and so is likely secondary. With a single exception (cobble W025k), all of the rest of the cobbles with non-hematite HT components from sites D111, D112, and W025/26 were completely demagnetized by 350 °C. These observed low unblocking temperatures are consistent with the dominance of pyrrhotite and goethite as indicated by our petrographic and rock magnetic data (Section 3). Note that we observed no systematic differences in cobble demagnetization with respect to cobble size, shape, sampling location, or core size.

Overall, these results are very different from those reported by Tarduno and Cottrell (2013), who reported highly stable, origin-trending characteristic high-temperature NRM components that unblocked from ~545 °C to 570–580 °C in 27 out of 28 cobbles and observed homogeneous NRM components within the 3 individual

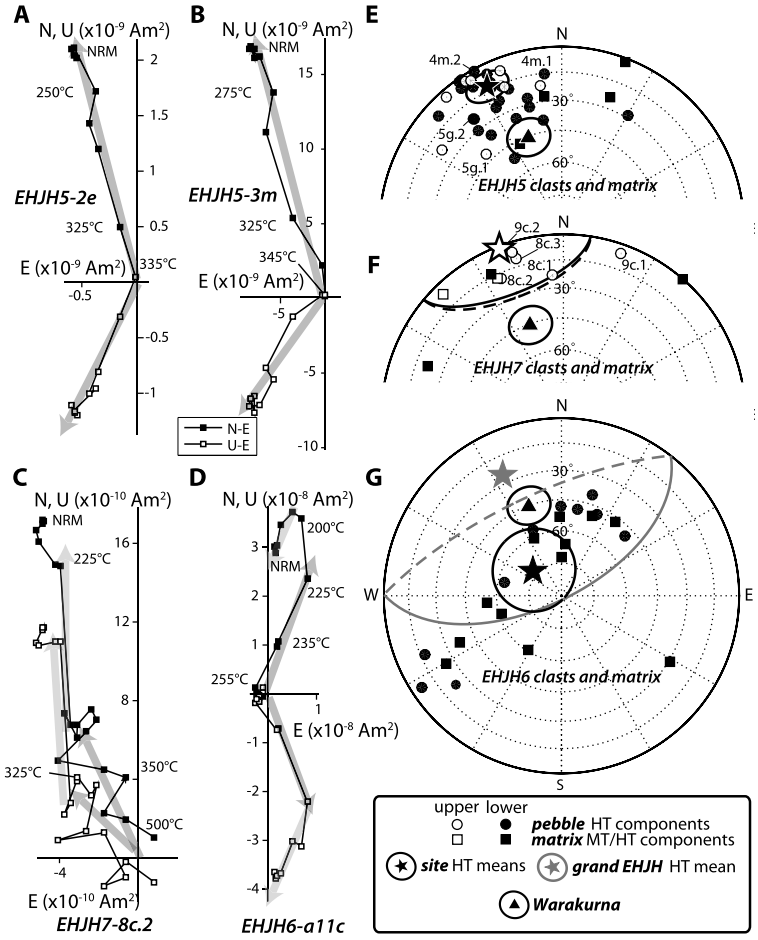

Fig. 9. Pebble conglomerate tests at Erawandoo Hill sites EHJH5, EHJH6, and EHJH7. (A–D) Two-dimensional projection of the endpoint of the NRM vector during AF and thermal demagnetization in geographic coordinates for clasts EHJH5-2e (A), EHJH5-3m (B), EHJH7-8c.2 (C), and EHJH6-a11c (D). Closed and open symbols represent end points of magnetization projected onto north–east (N–E) and up–east (U–E) planes, respectively. Temperatures for selected thermal demagnetization steps are labeled. LT and HT components are shown by light grey and dark grey arrows, respectively. (E–G) Equal area stereonet showing directions of magnetization components from clasts (circles) and matrix (squares) from sites EHJH5 (E), EHJH7 (F), and EHJH6 (G). For all clasts, HT components are shown, while for matrix, MT and HT components are shown for EHJH5 and EHJH7, respectively. Open and closed symbols represent upper and lower hemispheres. Stars and associated ellipses denote Fisher HT mean directions and associated 95% confidence ellipse for clasts at site EHJH5 (E) and combined clasts and matrix at sites EHJH7 and EHJH6 (F, G). Triangle and associated ellipse denotes local paleomagnetic field direction and 95% confidence interval for mean pole for Bangemall Supergroup sills (part of Warakurna LIP) (Wingate et al., 2002).

cobbles that they subsampled. We also do not see any evidence of a shallow southeast overprint observed in 20% of the samples reported by Tarduno and Cottrell (2013) (Fig. S6).

5. Implications

We find that the main remanence carrier in the Jack Hills quartzitic sediments is the low blocking temperature mineral pyrrhotite and, to a lesser extent, goethite. Therefore, with a few exceptions, we are only able to assess the remagnetization history in the sediments up to temperatures of ~330 °C (Table S3). Most of the remanence in the few sedimentary samples with higher NRM unblocking temperatures is carried by hematite, is oriented in the direction of the present local geomagnetic field, and is therefore likely of recent origin by oxidative weathering. On the other hand, the igneous rocks (monzogranite and dolerite) and several quartzitic samples contain abundant magnetite and record remagnetization up to unblocking temperatures of 580 °C (Table S3).

All three of our Erawandoo Hill pebble conglomerate tests failed, indicating complete remagnetization up to the maximum observed unblocking temperatures of 335–500 °C (Table S3). The mean remagnetization directions are close to that of a nearby 1078 Ma dolerite dyke and of the local geomagnetic field during the contemporaneous ~1070 Ma Warakurna LIP.

Furthermore, we found that clasts from the cobble conglomerates behave extremely unstably during laboratory demagnetization with unblocking temperatures almost exclusively <350 °C, nonlinear demagnetization trends that often do not reach origin-trending directions, and nonunidirectional magnetization directions within single cobbles. Such inhomogeneous and low-stability NRM can be produced by fine-scale aqueous alteration, weathering, and viscous remagnetization and invalidates the use of a conglomerate test for these samples. Furthermore, given the low unblocking temperatures of the cobble NRM, if these rocks experienced the same 350 °C–500 °C greenschist metamorphic event that affected the Erawandoo Hill rocks (Section 2), this would require that the cobbles' NRM postdates deposition.

Our cobble conglomerate test results contrast starkly with those of Tarduno and Cottrell (2013), who argued that the magnetizations of their clasts are dominantly carried by magnetite and who reported stable, origin-trending components that unblocked between 540 and 600 °C. The reasons for the great differences in ferromagnetic mineralogy and NRM between our two studies are unknown. It is conceivable that the two sample suites are simply lithologically distinct at the microscale (even though they appear similar at hand sample and outcrop scale). A second possibility is that the more stable NRM observed in Tarduno and Cottrell (2013)'s samples is the product of lightning-remagnetization. How-

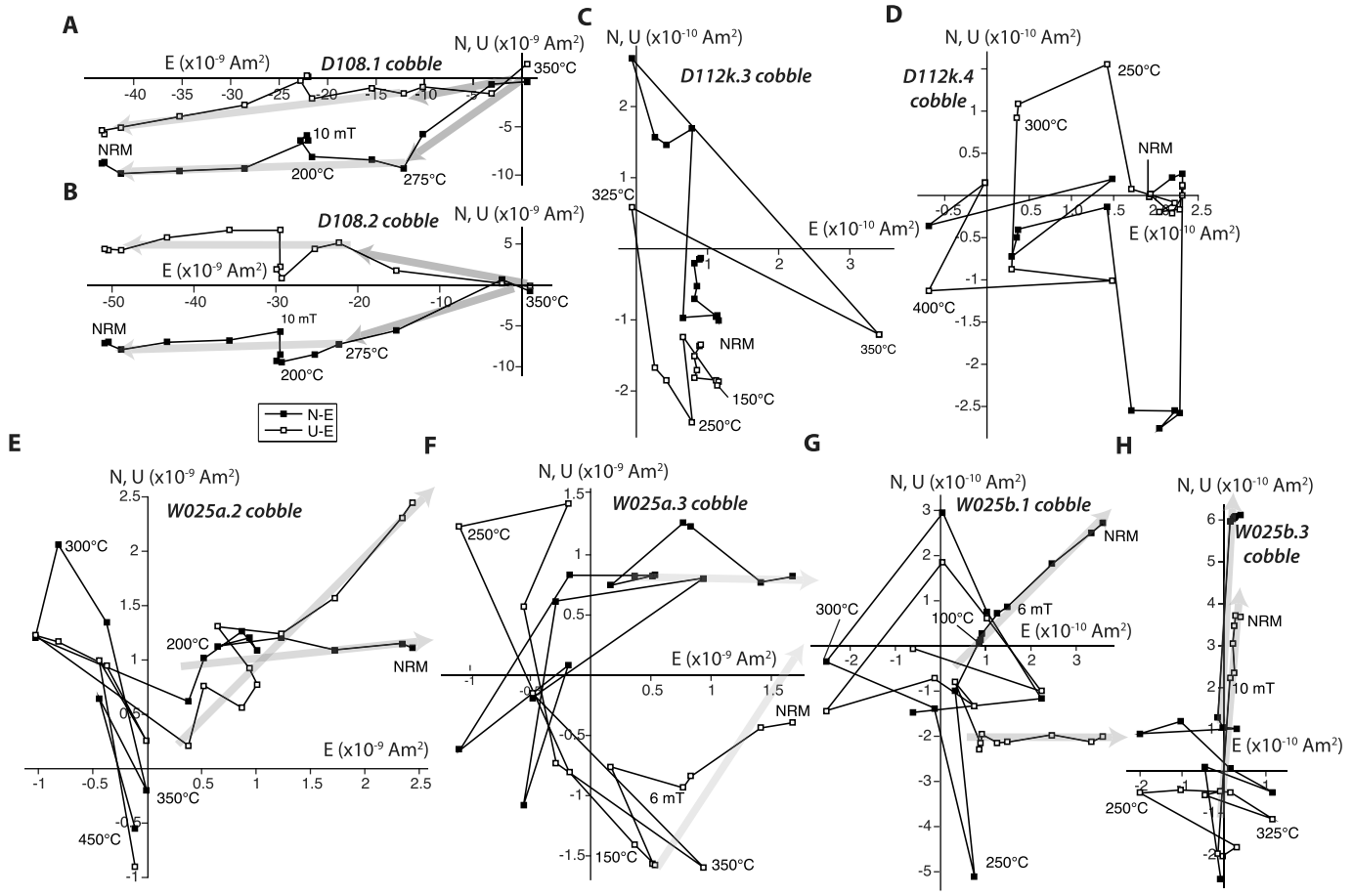

Fig. 10. Paleomagnetism of selected samples from the cobble conglomerate tests. Shown are two-dimensional projections of the endpoint of the NRM vector during AF and thermal demagnetization in geographic coordinates. Open and closed symbols represent end points of magnetization projected onto north–east (N–E) and up–east (U–E) planes, respectively. Peak AC fields and temperatures for selected AF and thermal demagnetization steps are labeled. Also shown are LC (lightest arrows), LT (intermediate shaded arrows) and HT (dark arrows) components. (A, B) Two subsamples from cobble D108 showing stable demagnetization and homogeneous components. (C, D) Two subsamples from cobble D112k showing unstable and inhomogeneous demagnetization behavior. (E, F) Two subsamples from cobble W025a showing unstable and inhomogeneous demagnetization behavior. (G, H) Two subsamples from cobble W025b showing unstable and inhomogeneous demagnetization behavior.

ever, both of these explanation are somewhat unsatisfying because they would require that by improbably low chance our samples suites are very different: among our 35 cobbles, we only observe a single cobble (D107g) with an NRM apparently partly carried by magnetite and three cobbles carrying highly stable NRM characteristic of lightning remagnetization, whereas all 28 of Tarduno and Cottrell (2013)'s cobbles have NRMs apparently dominated by magnetite. A third possibility is that our two sample suites have similar NRMs, but that subtle differences in laboratory methodology (i.e., sample contamination or alteration during heating) led to major differences in demagnetization behavior. Regardless, as discussed above, even if the positive conglomerate test of Tarduno and Cottrell (2013) is accepted, it would only confidently exclude remagnetization since 1.7 Ga (and possibly post-1.22 Ga), not since the Paleoarchean.

Our fold tests failed or were inconclusive, suggesting that the host rocks were likely remagnetized after the folding events. In particular, the site D197 rocks are remagnetized in the direction of the ∼1.1 Ga Warakurna LIP up to unblocking temperatures of 350 °C (Table S3). Associated with a local Warakurna dyke, all of our three baked contact tests were negative, with quartzite more than three dyke radii from the dyke center magnetized in the dyke's direction up to unblocking temperatures of at least 560–580 °C (Table S3). Furthermore, we have found that Erawandoo Hill pebble conglomerate samples from 0.2 km away, and even monzogranite up to at least 3 km away, are nearly completely magnetized in the dyke's direction up to unblocking temperatures of 500 °C and 580 °C, respectively.

With the exception of poles from the mid-Neoproterozoic (∼770 Ma), the dyke/Warakurna direction is distinct at >95% confidence from poles younger than 1070 Ma along Australia's apparent polar wander path (Swanson-Hysell et al., 2012; Torsvik et al., 2012), indicating that the remagnetization process was likely complete soon after dyke emplacement and is unlikely to be the product of a subsequent events unrelated to dyke emplacement. However, the peak temperature expected for county rock experiencing a purely thermal diffusive pulse from the intrusion of such a small dyke is insufficient to remagnetize rocks at such distal sites. We propose two alternative possible scenarios to account for these observations.

A first possibility is that regional-scale heating and/or hydrothermal alteration was generated by the magmatic activity from the Warakurna LIP, which is thought to have extended over much of west Australia at this time as the near-surface manifestation of a >1500 km diameter hot mantle plume head (Wingate et al., 2004). Numerous other dykes attributed to the Warakurna event have been identified throughout the Jack Hills (Spaggiari, 2007; Spaggiari et al., 2007) and northwest Yilgarn craton (Wingate et al., 2004). The fact that the monzogranite and some quartzitic rocks contain a magnetite-bearing HT component magnetized in the Warakurna LIP direction up to unblocking temperatures of 580 °C would seem to imply a total thermoremanent magnetization (TRM)

overprint from heating to at least 580 °C. However, such a high temperature appears to conflict with Ti-in-quartz and monazite–xenotime thermometry, which suggest peak metamorphic temperatures of ~346–487 °C. An alternative is that metamorphic temperatures from the Warakurna event were less than 580 °C and the monzogranite appears completely remagnetized due to the presence of multidomain grains with distributed unblocking temperatures approaching the magnetite Curie point (Dunlop and Özdemir, 1997). However, this would not readily explain the complete remagnetization of the small number of magnetite-bearing quartzitic rocks. A second alternative is that the Jack Hills was overprinted by a crystallization remanent magnetization (CRM) associated with aqueous alteration and metasomatism. In fact, it has been proposed that the presence of numerous epigenetic mineral deposits (including sulfide ores) throughout the Warakurna LIP region reflects a giant hydrothermal system at 1070 Ma (Pirajno, 2004; Wingate et al., 2004). Dissolution and reprecipitation of pyrrhotite and other sulfides is a common consequence of metasomatic processes in sediments (Hall, 1986), which could explain our observation that pyrrhotite is the dominant NRM carrier in our quartzite and conglomerate samples. In such a case, one cannot exclude the possibility that some inclusions armored within zircons might have escaped being aqueously remagnetized. However, this aqueous remagnetization scenario cannot readily account for the remagnetization of the monzogranite, whose characteristic NRM is dominated by magnetite.

A second scenario is that the local geomagnetic field direction at 2650 Ma was similar to that at 1070 Ma, such that intrusion of the monzogranite at the earlier time remagnetized much of the west-central Jack Hills in a direction coincidentally close to that of the dyke. We cannot exclude this scenario because the apparent polar wander path of the Narryer terrane is poorly constrained prior to 2418 Ma (Schmidt, 2014; Smirnov et al., 2013; Veikkolainen et al., 2014).

6. Conclusions

Our 12 field tests using 277 total subsamples from the area surrounding the Jack Hills Hadean-zircon bearing rocks at Erawandoo Hill yielded either negative outcomes, indicating complete remagnetization, or inconclusive results due to a lack of stable magnetization. These results include the first conglomerate tests directly on the Erawandoo Hill conglomerate. The bulk of the available evidence indicates that the Erawandoo Hill Hadean-zircon bearing pebble conglomerates, although largely free of the effects of lightning strikes, were pervasively remagnetized up to unblocking temperatures of at least 330 °C, and some nearby quartzites up to at least 580 °C. The source of this remagnetization was likely emplacement of the Warakurna LIP at 1070 Ma and/or the intrusion of monzogranite at 2650 Ma.

It is unclear whether the remagnetization process that affected the Jack Hills rocks was a TRM from heating or a CRM due to aqueous alteration. In the case of a TRM, the peak 580 °C unblocking temperatures of the Warakurna/dyke direction in most of the monzogranite samples and in selected quartzitic sediments may imply total thermal remagnetization of magnetite-bearing zircons in these and nearby rocks. However, such temperatures appear to conflict with some mineral thermometry estimates and therefore support at least some chemical remagnetization. In any case, even if it could eventually be established that the zircons have not been remagnetized completely since deposition at 2.65–3.05 Ga, the age of their magnetization would remain unconstrained for the missing 0.35–1.45 billion year rock record following their crystallization but predating the deposition of their host rocks.

Acknowledgements

We thank S. Mojzsis for introducing us to the Jack Hills in 2001, the Geological Survey of Western Australia for access to the Jack Hills Geoheritage Reserve, the residents and goat of Beringarra Station for logistical help, Crosslands Resources for showing us their iron ore mine, M. Wingate and R. Pidgeon for helpful discussions and logistical assistance, and D.A.D. Evans for helpful discussions on polar wander. We also thank M. Jackson from the Institute for Rock Magnetism and S. Ceballos, S. Bouma, and F. Hellman from U. C. Berkeley for assistance with magnetometry measurements, B. Carbone for administrative help, R. Bowens–Rubin for acquiring the EHJH5 measurements, and the NSF Early Concept Grants for Exploratory Research program grant EAR-1226293 for support. The UCLA ion microprobe facility is in part supported through a grant from NSF/EAR Instrument and Facilities Program. Partial support was also provided by the NASA Astrobiology Institute (grant NNA09DA80A to The New York Center for Astrobiology). We thank B. Buffett for editorial work and D.A.D. Evans and an anonymous reviewer for helpful reviews of the manuscript.

Appendix A. Supplementary material

Supplementary material related to this article can be found online at http://dx.doi.org/10.1016/j.epsl.2015.07.067.

References

Biggin, A., de Wit, M., Langereis, C., Zegers, T., Voute, S., Dekkers, M., Drost, K., 2011. Palaeomagnetism of Archaean rocks of the Onverwacht Group, Barberton Greenstone Belt (southern Africa): evidence for a stable and potentially reversing geomagnetic field at ca. 3.5 Ga. Earth Planet. Sci. Lett. 302, 314–328.

Buchan, K.L., 2007. Baked contact test. In: Gubbins, D., Herrero-Bervera, E. (Eds.), Encyclopedia of Geomagnetism and Paleomagnetism. Springer, Dordrecht, The Netherlands, pp. 35–39.

Cavosie, A.J., Wilde, S.A., Liu, D., Weiblen, P.W., Valley, J.W., 2004. Internal zoning and U–Th–Pb chemistry of Jack Hills detrital zircons: a mineral record of early Archean to Mesoproterozoic (4348–1576 Ma) magmatism. Precambrian Res. 135, 251–279.

Cherniak, D.J., Watson, E.B., 2000. Pb diffusion in zircon. Chem. Geol. 172, 5–24.

Dekkers, M.J., 1989. Magnetic properties of natural goethite-II. TRM behaviour during thermal and alternating field demagnetization and low-temperature treatment. Geophys. J. 97, 341–355.

Dunlop, D.J., Özdemir, O., 1997. Rock Magnetism: Fundamentals and Frontiers. Cambridge University Press, New York. 573 pp.

Dunn, S.J., Nemchin, A.A., Cawood, P.A., Pidgeon, R.T., 2005. Provenance record of the Jack Hills metasedimentary belt: source of the Earth's oldest zircons. Precambrian Res. 138, 235–254.

Eriksson, K.A., Wilde, S.A., 2010. Palaeoenvironmental analysis of Archaean siliciclastic sedimentary rocks in the west–central Jack Hills belt, Western Australia with new constraints on ages and correlations. J. Geol. Soc. (Lond.) 167, 827–840.

Gomi, H., Ohta, K., Hirose, K., Labrosse, S., Caracas, R., Verstraete, M.J., Hernlund, J.W., 2013. The high conductivity of iron and thermal evolution of the Earth's core. Phys. Earth Planet. Inter. 224, 88–103.

Graham, J.W., 1949. The stability and significance of magnetism in sedimentary rocks. J. Geophys. Res. 54, 131–167.

Grange, M.L., Wilde, S.A., Nemchin, A.A., Pidgeon, R.T., 2010. Proterozoic events recorded in quartzite cobbles at Jack Hills, Western Australia: new constraints on sedimentation and source of >4 Ga zircons. Earth Planet. Sci. Lett. 292, 158–169.

Gubbins, D., Alfè, D., Masters, G., Price, D., Gillan, M., 2004. Gross thermodynamics of two-component core convection. Geophys. J. Int. 157, 1407–1414.

Hall, A.J., 1986. Pyrite-pyrrhotine redox reactions in nature. Mineral. Mag. 50, 223–229.

Holden, P., Lanc, P., Ireland, T.R., Harrison, T.M., Foster, J.J., Bruce, Z., 2009. Mass-spectrometric mining of Hadean zircons by automated SHRIMP multi-collector and single-collector U/Pb zircon age dating: the first 100 000 grains. Int. J. Mass Spectrom. 286, 53–63.

Jaeger, J.C., 1964. Thermal effects of intrusions. Rev. Geophys. 2, 443–466.

Kirschvink, J.L., 1980. The least-squares line and plane and the analysis of paleomagnetic data: examples from Siberia and Morocco. Geophys. J. R. Astron. Soc. 62, 699–718.

Kirschvink, J.L., Kopp, R.E., Raub, T.D., 2008. Rapid, precise, and high-sensitivity acquisition of paleomagnetic and rock-magnetic data: development of a low-noise automatic sample changing system for superconducting rock magnetometers. Geochem. Geophys. Geosyst. 9, Q05Y01. http://dx.doi.org/10.1029/2007GC001856.

Lammer, H., Kasting, J.F., Chassefière, E., Johnson, R.E., Kulikov, Y.N., Tian, F., 2008. Atmospheric escape and evolution of the terrestrial planets and satellites. Space Sci. Rev. 139, 399–436.

Lowrie, W., 1990. Identification of ferromagnetic minerals in a rock by coercivity and unblocking temperature properties. Geophys. Res. Lett. 17, 159–162.

Maas, R., Kinny, P.D., Williams, I.S., Froude, D.O., Compston, W., 1992. The Earth's oldest known crust: a geochronological and geochemical study of 3900–4200 Ma old detrital zircons from Mt. Narryer and Jack Hills, Western-Australia. Geochim. Cosmochim. Acta 56, 1281–1300.

McElhinny, M.W., 1964. Statistical significance of the fold test in paleomagnetism. Geophys. J. R. Astron. Soc. 8, 338–340.

Mezger, K., Krogstad, E.J., 1997. Interpretation of discordant U–Pb zircon ages: an evaluation. J. Metamorph. Geol. 15, 127–140.

Nimmo, F., Price, G.D., Brodholt, J., Gubbins, D., 2004. The influence of potassium on core and geodynamo evolution. Geophys. J. Int. 156, 363–376.

Özdemir, Ö., Dunlop, D.J., 1996. Thermoremanence and Néel temperature of goethite. Geophys. Res. Lett. 23, 921–924.

Pidgeon, R.T., Wilde, S.A., 1998. The interpretation of complex zircon U–Pb systems in Archaean granitoids and gneisses from the Jack Hills, Narryer Gneiss Terrane, Western Australia. Precambrian Res. 91, 309–322.

Pirajno, F., 2004. Metallogeny in the Capricorn Orogen, Western Australia, the result of multiple ore-forming processes. Precambrian Res. 128, 411–439.

Rasmussen, B., Fletcher, I.R., Muhling, J.R., Wilde, S.A., 2010. In situ U–Th–Pb geochronology of monazite and xenotime from the Jack Hills belt: implications for the age of deposition and metamorphism of Hadean zircons. Precambrian Res. 180, 26–46.

Rasmussen, B., Fletcher, I.R., Muhling, J.R., Gregory, C.J., Wilde, S.A., 2011. Metamorphic replacement of mineral inclusions in detrital zircon from Jack Hills, Australia: implications for the Hadean Earth. Geology 39, 1143–1146.

Schmidt, P.W., 2014. A review of Precambrian palaeomagnetism of Australia: palaeogeography, supercontinents, glaciations and true polar wander. Gondwana Res. 25, 1164–1185.

Smirnov, A.V., Evans, D.A.D., Ernst, R.E., Söderlund, U., Li, Z.-X., 2013. Trading partners: tectonic ancestry of southern Africa and western Australia, in Archean supercratons Vaalbara and Zimgarn. Precambrian Res. 224, 11–22.

Spaggiari, C.V., 2007. The Jack Hills greenstone belt, Western Australia Part 1: structural and tectonic evolution over >1.5 Ga. Precambrian Res. 155, 204–228.

Spaggiari, C.V., Pidgeon, R.T., Wilde, S.A., 2007. The Jack Hills greenstone belt, Western Australia Part 2: lithological relationships and implications for the deposition of ≥4.0 Ga detrital zircons. Precambrian Res. 155, 261–286.

Spaggiari, C.V., Wartho, J.-A., Wilde, S.A., 2008. Proterozoic deformation in the northwest of the Archean Yilgarn Craton, Western Australia. Precambrian Res. 162, 354–384.

Swanson-Hysell, N.L., Feinberg, J.M., Berquó, T.S., Maloof, A.C., 2011. Self-reversed magnetization held by martite in basalt flows from the 1.1-billion-year-old Keweenawan rift, Canada. Earth Planet. Sci. Lett. 305, 171–184.

Swanson-Hysell, N.L., Maloof, A.C., Kirschvink, J.L., Evans, D.A.D., Halversong, G.P., Hurtgen, M.T., 2012. Constraints on Neoproterozoic paleogeography and Paleozoic orogenesis from paleomagnetic records of the Bitter Springs formation, Amadeus Basin, Central Australia. Am. J. Sci. 312, 817–884.

Tarduno, J.A., Cottrell, R.D., Watkeys, M., Hofmann, A., Doubrovine, P.V., Mamajek, E.E., Liu, D., Sibeck, D.G., Neukirch, L.P., Usui, Y., 2010. Geodynamo, solar wind, and magnetopause 3.4 to 3.45 billion years ago. Science 327, 1238–1240.

Tarduno, J.A., Cottrell, R.D., 2013. Signals from the ancient geodynamo: a paleomagnetic field test on the Jack Hills metaconglomerate. Earth Planet. Sci. Lett. 367, 123–132.

Tarduno, J.A., Blackman, E.G., Mamajek, E.E., 2014. Detecting the oldest geodynamo and attendant shielding from the solar wind: implications for habitability. Phys. Earth Planet. Inter. 233, 68–87.

Torsvik, T.H., Van der Voo, R., Preeden, U., Mac Niocaill, C., Steinberger, B., Doubrovine, P.V., van Hinsbergen, D.J.J., Domeier, M., Gaina, C., Tohver, E., Meert, J.G., McCausland, P.J.A., Cocks, L.R.M., 2012. Phanerozoic polar wander, palaeogeography and dynamics. Earth-Sci. Rev. 114, 325–368.

Veikkolainen, T., Pesonen, L.J., Evans, D.A.D., 2014. PALEOMAGIA: a PHP/MYSQL database of the Precambrian paleomagnetic data. Stud. Geophys. Geod. 58, 425–441.

Watson, G.S., 1956. A test for randomness. Mon. Not. R. Astron. Soc. 7, 160–161.

Wilde, S.A., Pidgeon, R.T., 1990. Geology of the Jack Hills metasedimentary rocks. In: Ho, S.E., Glover, J.E., Myers, J.S., Muhling, J.R. (Eds.), Third International Archaean Symposium (Perth) Excursion Guidebook, vol. 21. University of Western Australia Extension Publication, Perth, pp. 82–95.

Wilde, S.A., 2010. Proterozoic volcanism in the Jack Hills Belt, Western Australia: some implications and consequences for the World's oldest zircon population. Precambrian Res. 183, 9–24.

Wingate, M.T.D., Pisarevsky, S.A., Evans, D.A.D., 2002. Rodinia connections between Australia and Laurentia: no SWEAT, no AUSWUS? Terra Nova 14, 121–128.

Wingate, M.T.D., Pirajno, F., Morris, P.A., 2004. Warakurna large igneous province: a new Mesoproterozoic large igneous province in west-central Australia. Geology 32, 105–108.

Ziegler, L.B., Stegman, D.R., 2013. Implications of a long-lived basal magma ocean in generating Earth's ancient magnetic field. Geochem. Geophys. Geosyst. 14. http://dx.doi.org/10.1002/2013GC005001.

Supplementary Material for

B. P. Weiss et al. (2015) Pervasive Remagnetization of Detrital Zircon Host Rocks in the Jack Hills, Western Australia and Implications for Records of the Early Geodynamo, *Earth Planet Sci. Lett.*

A. Thermal and deformational events in the Jack Hills

There were at least three major phases of metamorphism and deformation that affected the association 3 rocks of the Jack Hills. The first major event is thought to be associated with the collision of the Narryer terrane with the adjacent Younami terrane (Myers, 1995), estimated to be complete by ~2600 Ma. Evidence for this event includes intrusive contacts between 2654 ± 7 Ma monzogranite (Pidgeon and Wilde, 1998) and associations 1 and 2 and 2654 ± 5 Ma U-Pb ages for metamorphic monazite in the matrix of Erawandoo Hill pebble conglomerate and as inclusions in Erawandoo Hill detrital zircons. Monazite-xenotime thermometry on Erawandoo Hill samples indicates temperatures reached ~430-470°C at 2653 ± 5 Ma, consistent with 346-487°C temperatures estimated using Ti-in-quartz thermometry (Rasmussen et al., 2010). Thus, although the intrusive contacts between association 3 rocks and the monzogranite are unclear, it is clear that the intrusion postdated deposition of, and by implication metamorphosed, the Erawandoo Hill conglomerate and is likely responsible for the observed greenschist facies mineralogy.

The second event is thought to be associated with the Glenburgh orogeny (collision of Pilboyne and Yilgarn cratons) at 1960-2005 Ma, manifested as inferred 300-500°C thermal disturbances of hornblende and muscovite $^{40}Ar/^{39}Ar$ age spectra (Spaggiari et al., 2008). The third event is thought to be associated with the Capricorn orogeny (intracratonic working of the West Australia craton), manifested as large-scale east–west-trending dextral shearing, 1738-1828 Ma $^{40}Ar/^{39}Ar$ muscovite and biotite ages throughout much of the Jack Hills (Spaggiari et al., 2008), and 1820 ± 25 Ma U-Pb ages for secondary xenotime in association 1 rocks (Rasmussen et al., 2010). Later lower grade disturbances of unknown ages are manifested as kink and conjugate-style folding, faulting and fault reactivation (Spaggiari, 2007).

The last phases of major metamorphism are thought to be associated with the intrusion of dykes associated with the Marnda Moorn and Warakurna large igneous provinces (LIPs) at ~1210 and ~1070 Ma, respectively (Wang et al., 2014; Wingate et al., 2004). Evidence for the latter disturbances include 1130 ± 130 radiation damage ages for Erawandoo Hill detrital zircons (Pidgeon, 2014) [indicating peak temperatures of at least 230 ± 25°C], 980 ± 150 Ma U-Pb discordia lower intercept ages for Jack Hills monzogranite (Pidgeon, 1992), and muscovite $^{40}Ar/^{39}Ar$ laser probe ages indicating a disturbance at ≤1172 Ma (Spaggiari et al., 2008). A final disturbance at ~800 Ma has been recognized from U-Pb ages of monazite and xenotime in the Erawandoo Hill conglomerate (Rasmussen et al., 2010; Rasmussen et al., 2011).

B. Additional rock magnetic experiments.

B.1. High-temperature low-field susceptibility. We measured temperature-dependent susceptibility for powders generated from six cobble clasts in a field of 0.9 mT from room-temperature up to temperatures as high as 700°C. Cobbles were heated in either air or Ar up to various peak temperatures, with some subsamples subjected to multiple heating and cooling cycles to progressively higher peak temperatures. All measurements were acquired with an AGICO MFK1-FA Kappabridge in the UC Santa Cruz Paleomagnetism Laboratory.

During our Kappabridge experiments conducted in air, only one of the six cobbles (D112l) exhibited susceptibility well above the instrument noise limit. For this sample, we observed a susceptibility peak during warming at ~500°C followed by a prominent drop in susceptibility around the magnetite Curie point (compare Fig. 3A with 3C, F and Fig. S1D). The rise and fall in susceptibility during warming and much higher susceptibility during cooling suggests that much of this magnetite was produced by oxidation during the experiment, possibly from sulfides as has been previously observed (Li and Zhang, 2005; Tudryn and Tucholka, 2004; Wang et al., 2008). Cobbles D112k, D112l and W026 also exhibited a small drop in remanence around the hematite Néel point in both air and Ar (Fig. 3A, B, F and Fig. S1B, C). We observed no indication of pyrrhotite's Néel temperature in susceptibility measurements of any sample.

These results differ from the cobble susceptibility measurements by Tarduno and Cottrell (2013). For most of their samples, heating in air led to a pronounced drop in susceptibility around the magnetite Curie point and only mild irreversibility; by comparison only one of our samples showed a strong susceptibility signal in air, while this sample altered significantly (Fig. 3A). Although two of Tarduno and Cottrell (2013)'s other samples did show susceptibility peaks around the magnetite Curie point and irreversibility similar to the results of our Ar heating experiments (Fig. 3E, G and Fig. S1D), their heating experiments in Ar produced susceptibility peaks around pyrrhotite's Curie point (unlike the production of magnetite observed in our Ar experiments; e.g., Fig. 3B, E, G). These results collectively suggest that unlike the cobbles of Tarduno and Cottrell (2013), our fresh cobbles have significant quantities of hematite and goethite and much less magnetite.

B.2. Low-temperature saturation remanence. Low temperature cycling experiments were conducted on fresh cobbles as well as subsamples of cobbles previously subjected to the Kappabridge high-temperature susceptibility measurements. Samples were exposed to a 5 T pulse field at room temperature and then cycled down to 20 K and back up to room temperature in a near-zero field environment using a Magnetic Properties Measurement System (MPMS) 2 equipped with the ultra low field option at the Institute of Rock Magnetism, U. Minnesota.

Our low-temperature cycling of fresh cobble sample D112l identified the 32 K Besnus transition diagnostic of monoclinic pyrrhotite as well as a weaker ~120 K Verwey transition diagnostic of near-stoichiometric magnetite [see (Dunlop and Özdemir, 1997)] (Fig. 3E). However, low-temperature cycling of D112l subsamples previously been heated in air and Ar showed that the Besnus transition had been destroyed while the 120 K transition was strongly enhanced (Fig. 3F), with the remanence having increased by an order of magnitude. These results provide more evidence that the Kappabridge measurements altered the samples leading to the production of magnetite and additionally show that pyrrhotite was destroyed. Given the abundance of pyrrhotite and the paucity of magnetite in these samples as indicated by the MPMS measurements, thermal demagnetization of IRM (main text Section 3.2), and electron microscopy (main text Section 3.4), it is clear that high-temperature susceptibility experiments are insensitive to the presence of pyrrhotite relative to magnetite in the Jack Hills cobbles.

B.3. Room temperature hysteresis and back field isothermal remanence (IRM). Hysteresis measurements were acquired with a Lakeshore Model 668 Vibrating Sample Magnetometer (VSM) in the laboratory of F. Hellman at UC Berkeley. Many samples exhibited strong paramagnetic behavior; the high-field slope of each hysteresis loop was used to estimate the

contribution of paramagnetic and diamagnetic minerals and isolate the ferromagnetic components (Fig. S3).

A Dunlop-Day plot (Dunlop, 2002) suggests that the mean grain sizes of the samples ranges from pseudo single domain to single domain. Although this plot is useful for characterizing most of the samples, it is likely misleading for the monzogranites. Although the plot suggests that the monzogranites contain mixtures of single domain and superparamagnetic grains, the wasp-waisted shapes of their hysteresis loops (Fig. S3D) and their low S-ratios (the IRM in a backfield of 0.3 T divided by IRM acquired in 1.5 T field) of 0.11-0.54, along with the evidence for magnetite, hematite and goethite in monzogranite thermal demagnetization of IRM data (Figs. 2A and S1A), suggest that they are instead likely mixtures of multidomain magnetite and single domain hematite and goethite [see Roberts et al. (1995)].

C. U-Pb geochronology

C.1. Sample and methods

Prismatic zircon crystals were separated from a sample of Erawandoo Hill dolerite (sample Dol6) by standard heavy mineral separation techniques using high-density liquids. Dolerite zircons had undergone variable degrees of metamictization due to sustained radiation damage, as manifested by their turbid colors (Fig. S4) and physical fragility. Four single zircons were selected based on grain morphology and clarity, and analyzed by the U-Pb isotope dilution thermal-ionization mass spectrometry (ID-TIMS) technique following the general procedures described in Ramezani et al. (2011). All zircons were pre-treated prior to dissolution by a chemical abrasion (CA-TIMS) method modified after Mattinson (2005) to mitigate the effects of radiation-induced Pb loss, and were subsequently spiked with the EARTHTIME ET535 mixed ^{205}Pb-^{233}U-^{235}U tracer prior to dissolution and analysis. Chemical abrasion involved thermal annealing of zircons in a furnace at 900°C for 60 hours, followed by leaching in concentrated HF at 180°C for 5 hours. Because of significant metamictization, the Dol6 zircons would not withstand the more intensive leach schedule typically applied to Phanerozoic zircons (11 to 13 hours at 210°C). Isotopic measurements of U and Pb were made on a VG Sector 54 multi-collector mass spectrometer equipped with a Daly ion-counting system. Data reduction including date calculation and propagation of uncertainties was carried out using computer applications and algorithms of Bowring et al. (2011) and McLean et al. (2011). Complete U-Pb data appear in Table S1.

For Mesoproterozoic and older zircons, the generally high precision of the ^{207}Pb/^{206}Pb dates (relative to the corresponding Pb/U dates) and their relative insensitivity to modern Pb loss renders them reliable estimates of the zircon crystallization age. The estimation of a crystallization age for this sample is thus based on the weighted mean ^{207}Pb/^{206}Pb date of a coherent cluster of zircon analyses for which dispersion in the data can be explained by analytical uncertainties alone. Weighted mean date uncertainties are reported at 95% confidence level and follow the notation ±X/Y/Z Ma, where X is the internal (analytical) uncertainty in the absence of all external errors, Y incorporates the U-Pb tracer calibration error and Z includes the latter as well as the decay constant errors of Jaffey et al. (1971). Incorporation of tracer calibration error (Y) is necessary for comparison between data from different techniques, such as ID-TIMS versus sensitive high-resolution ion microprobe (SHRIMP).

C.2. Results

Four zircons analyzed from sample Dol6 yield a discordant array with $^{206}Pb/^{238}U$ dates that range from 1069.59 ± 0.99 Ma to 1079.7 ± 3.0 Ma (Fig. S5) and are likely best explained by variable degrees of Pb loss (see above). Nevertheless, their $^{207}Pb/^{206}Pb$ dates yield a weighted mean of 1078.4 ± 3.4/4.4/6.6 Ma and a MSWD of 0.036. This date represents the best estimate for the emplacement of the dolerite dyke within the supracrustal rocks. The emplacement age of the Erawandoo Hill dolerite overlaps with the estimates for the timing of magmatism associated with the Warakurna large igneous province in west-central Australia (1052 ± 11 to 1078 ± 5 Ma) based on SHRIMP U-Pb zircon geochronology (Wingate et al., 2004).

D. More details about component naming

The component names were assigned based on the range of observed demagnetization temperatures and coercivities in a given sample. Because we are using this notation for components from a diversity of sample lithologies from around the Jack Hills, components with the same name but identified at different sites may not always have the same direction and origin. For example, monzogranite HT components (Section 4.3) persist during thermal demagnetization to several hundred °C higher temperatures and have different directions from HT components identified from the cobble conglomerates (Section 5.2), indicating a different remanence carrier. Furthermore, components with the same name from a single site may even have a diverse origin, particularly for the cobble conglomerate samples for which little stable NRM was observed.

Supplementary Figures

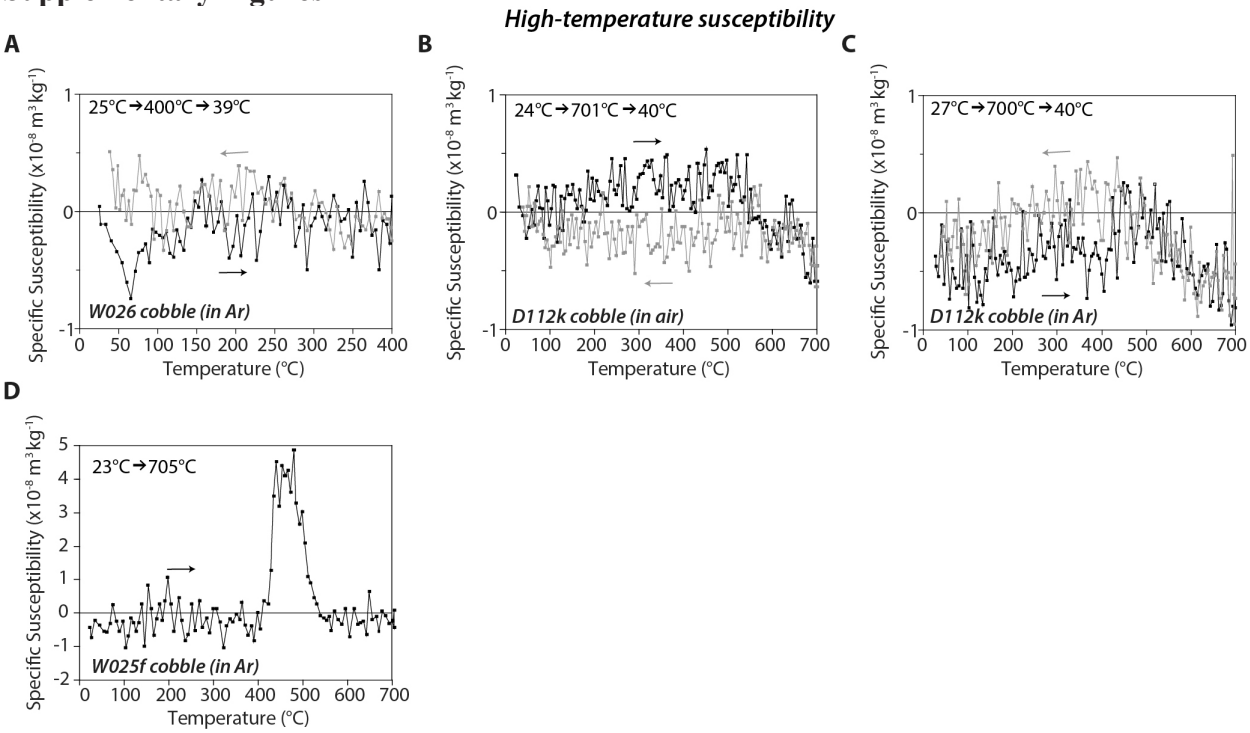

Fig. S1. High temperature susceptibility data. (A) W026 cycled in Ar cycled up to 400°C. (B) D112k cycled in air cycled up to 701°C. (B) D112k cycled in Ar cycled up to 700°C. (D) W025f cycled in Ar cycled up to 705°C.

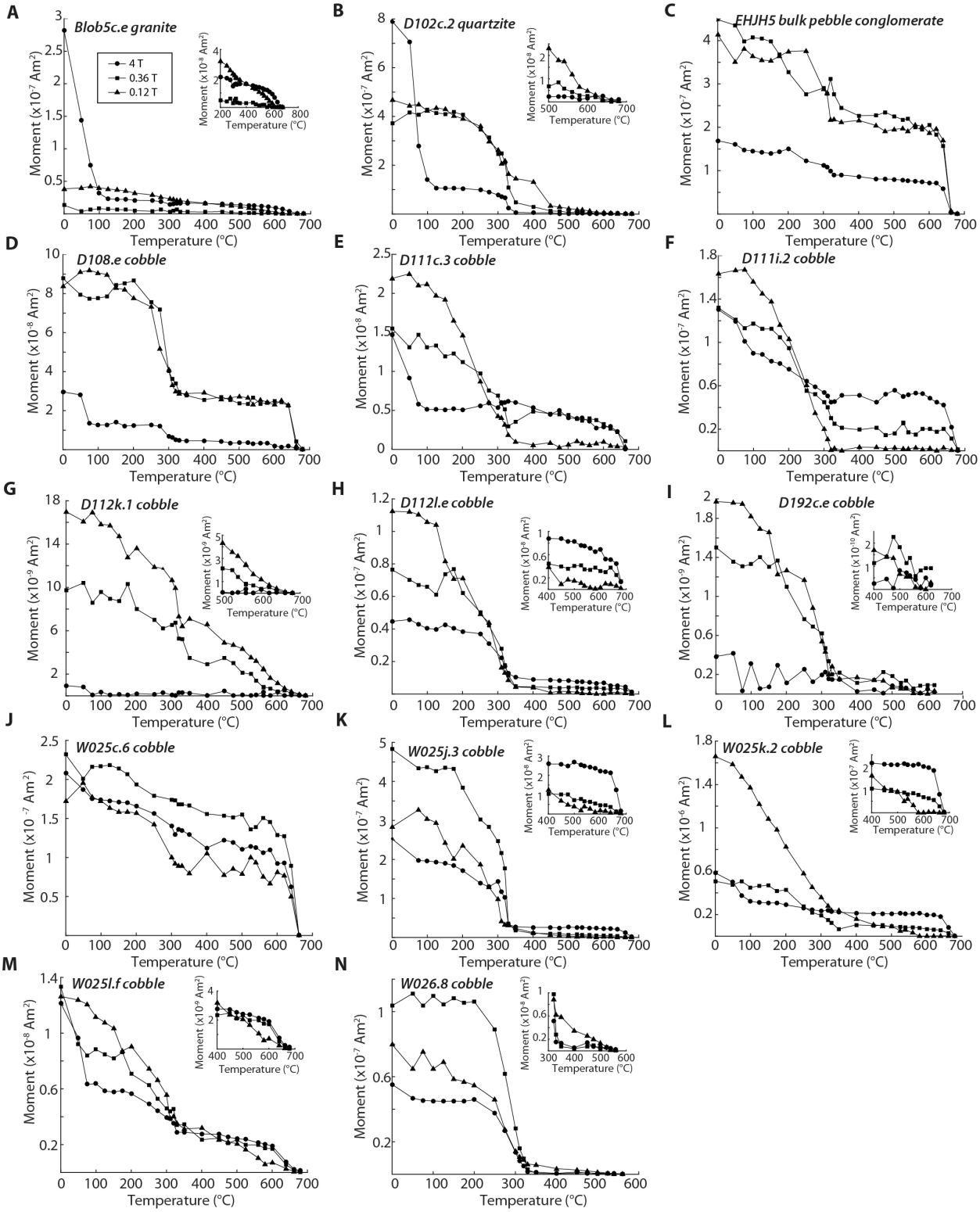

Fig. S2. More examples of thermal demagnetization of a three-component IRM produced by magnetizing the sample in a 4 T field along the *z*-axis, followed by 0.36 T along the north *x*-axis, and 0.12 T along the *y*-axis. Each plot contains curves showing the corresponding *z*- (circles), *y*- (squares), and *x*- (triangles) magnetization components. (A) Granite sample Blob5c.e. (B) Quartzitic fold test sample D102c.2. (C) Bulk sample (clast and matrix) from Erawandoo Hill

pebble conglomerate EHJH5. (D) Clast from cobble conglomerate D108.e. (E) Clast from cobble conglomerate D111c.3. (F) Clast from cobble conglomerate D111i.2 (G) Clast from cobble conglomerate D112k.1. (H) Clast from cobble conglomerate D112l.e. (I) Clast from cobble conglomerate D192c.e. (J) Clast from cobble conglomerate W025c.6. (K) Clast from cobble conglomerate W025j.3. (L) Clast from cobble conglomerate W025k.2. (M) Clast from cobble conglomerate W025l.f. (N) Clast from cobble conglomerate W026.

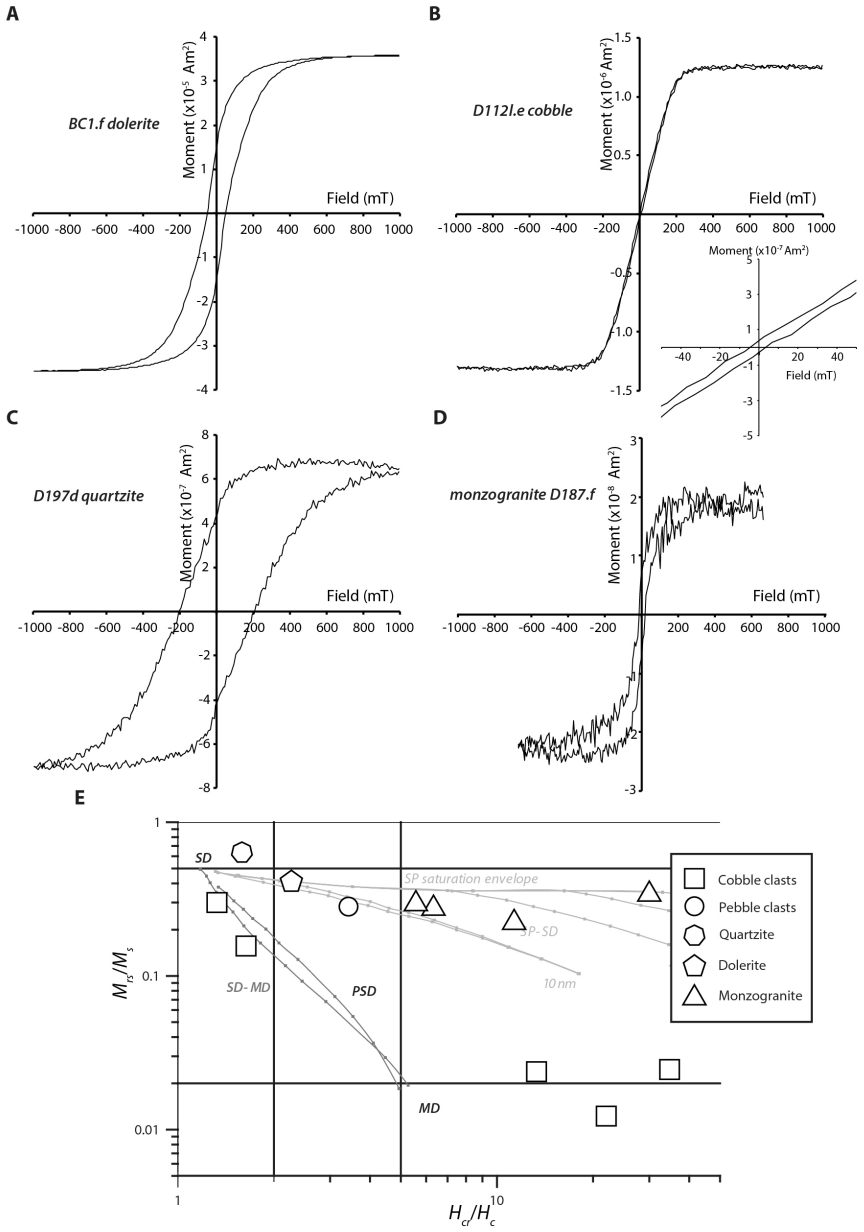

Fig. S3. Room-temperature hysteresis properties of selected samples. (A-D) Room temperature hysteresis loops for dolerite BC1.f (A), clast from cobble conglomerate D112l.e (B), quartzite from fold test D197d (C), and monozogranite D187.f (D). Paramagnetic contributions have been removed from these loops. (E) Dunlop-Day plot (Dunlop, 2002) showing the ratio of coercivity of remanence to coercivity (H_{cr}/H_c) versus the ratio of saturation remanence to saturation magnetization (M_{rs}/M_s) for all samples that yielded low-noise hysteresis loops. Single domain

(SD), pseudo single domain (PSD) and multidomain (MD) ranges calculated for magnetite are indicated, as well as mixing lines between SD and MD and between SD and superparamagnetic (SP) of different sizes are also indicated. Lithologies of samples are denoted by squares for cobbles, circles for pebbles, heptagons for quartzite, pentagons for dolerite, and triangles for monzogranite.

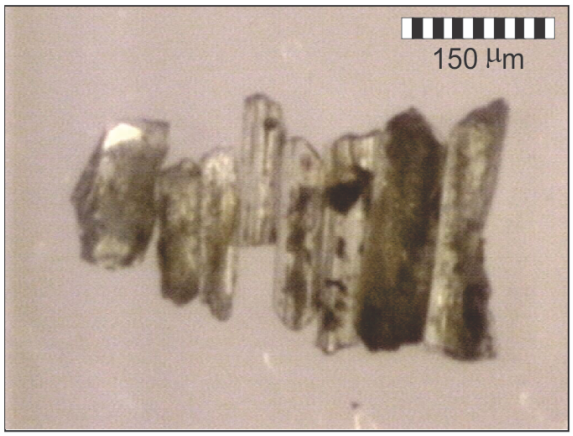

Fig. S4. Photomicrograph of selected zircon grains for U-Pb analysis from dolerite sample Dol6.

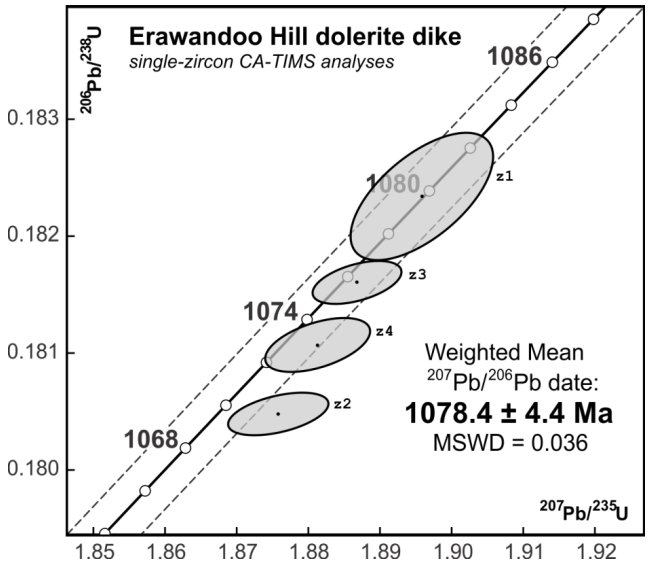

Fig. S5. U-Pb concordia plot for Dol6 dolerite sample with individual analyses of zircon shown with 2σ error ellipses. Uncertainty of the weighted mean date includes all sources of internal (analytical) error as well as the U-Pb tracer calibration error, reported at 95% confidence. Dashed lines mark the concordia error envelope. Complete U-Pb isotopic data are reported in Table S1. MSWD is mean square of weighted deviates.

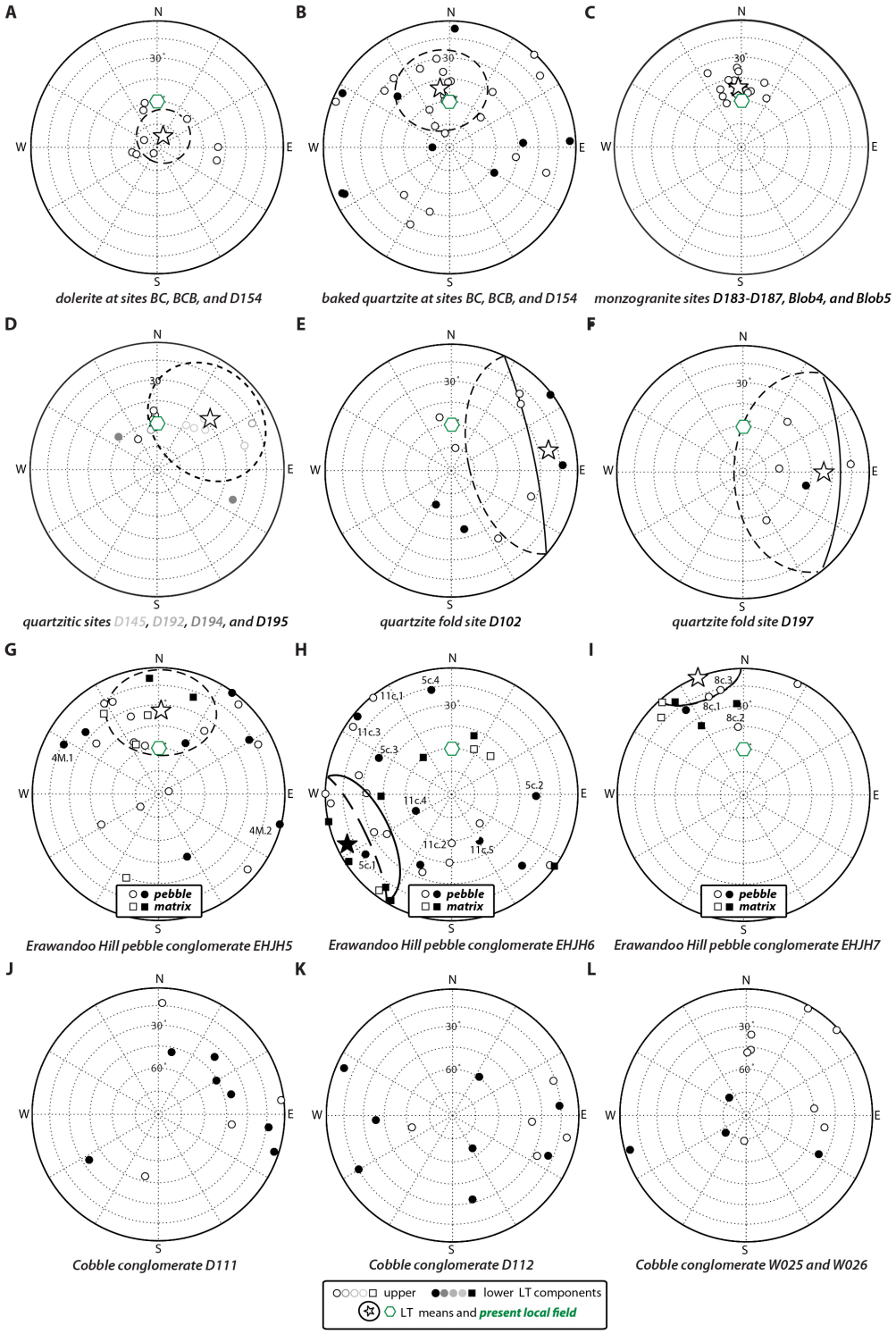

Fig. S6. Equal area stereonets showing LT components. Open and closed symbols represent upper and lower hemispheres. Stars and associated ellipses denote Fisher LT mean directions and associated 95% confidence ellipses for each plot. Green hexagon denotes local geomagnetic field direction. (A) Dolerite at baked contact test sites BC, BCB, and D154. (B) Quartzite at dolerite baked contact test sites BC, BCB, and D154. (C) Monzogranite at sites D183-D187, Blob4, and Blob5. (D) Quartzite at site D145, D192, D194, and D195. (E) Quartzite at fold test

site D102. (F) Quartzite at fold test site D197. (G) Clasts and matrix from Erawandoo Hill pebble conglomerate EHJH5. (H) Clasts and matrix from Erawandoo Hill pebble conglomerate EHJH6. (I) Clasts and matrix from Erawandoo Hill pebble conglomerate EHJH7. (J) Clasts from cobble conglomerate at site D111. (K) Clasts from cobble conglomerate at site D112. (L) Clasts from cobble conglomerate at sites W025 and W026. In (G-I), circles represent clasts and squares represent matrix.

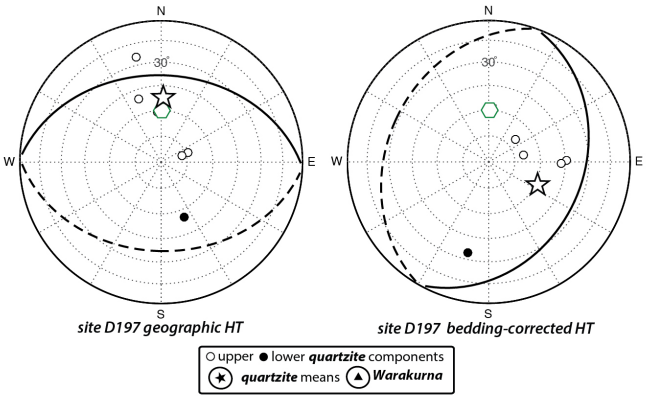

Fig. S7. Equal area stereonets showing HT directions isolate from quartzite samples at fold test site D197 in (A) geographic coordinates and (B) bedding-corrected coordinates. Open and closed symbols represent upper and lower hemispheres. Stars and associated ellipses denote Fisher LT mean directions and associated 95% confidence ellipses for each plot. The mean values do not assume auto-reversal of the one reversed sample. Hexagon denotes local geomagnetic field direction.

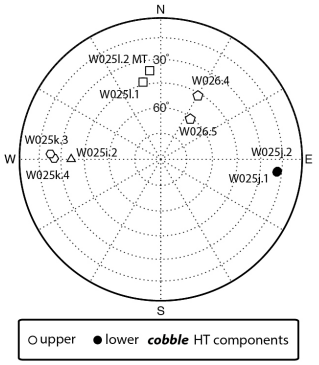

Fig. S8. Equal area stereonet showing HT directions for all W025 and W026 cobbles that yielded linear, origin-trending characteristic components. Subsamples from the same clast are denoted with the same symbol. Open and closed symbols represent upper and lower hemispheres.

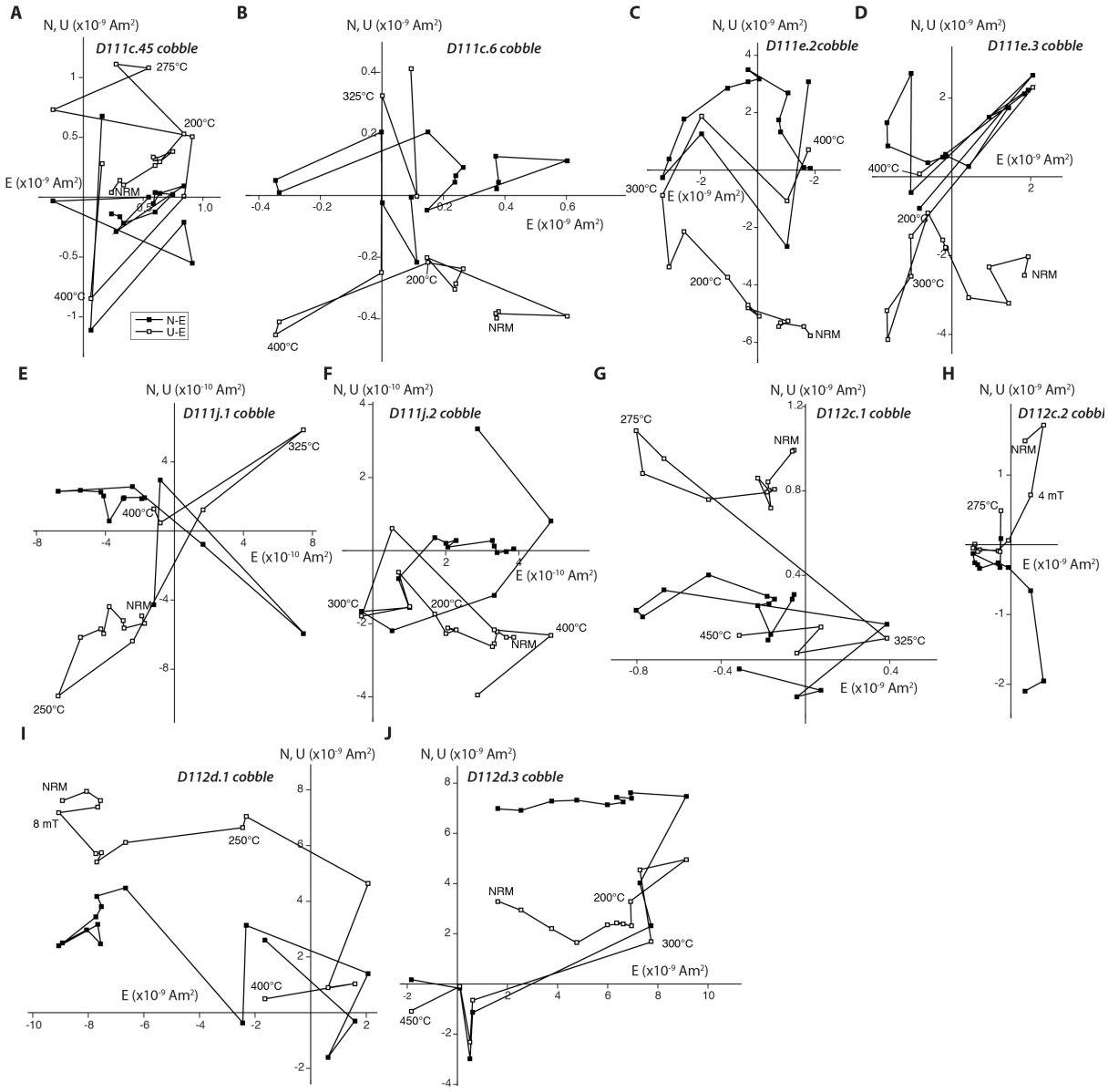

Fig. S9. Paleomagnetism of additional samples from the cobble conglomerate tests. Shown are two-dimensional projections of the endpoint of the NRM vector during AF and thermal demagnetization in geographic coordinates. Open and closed symbols represent end points of magnetization projected onto north-east (N-E) and up-east (U-E) planes, respectively. Peak AC fields and temperatures for selected AF and thermal demagnetization steps are labeled. (A, B) Two subsamples from cobble D111c. (C, D) Two subsamples from cobble D111e. (E, F) Two subsamples from cobble D111j. (G, H) Two subsamples from cobble D112c. (I, J) Two subsamples from cobble D112d.

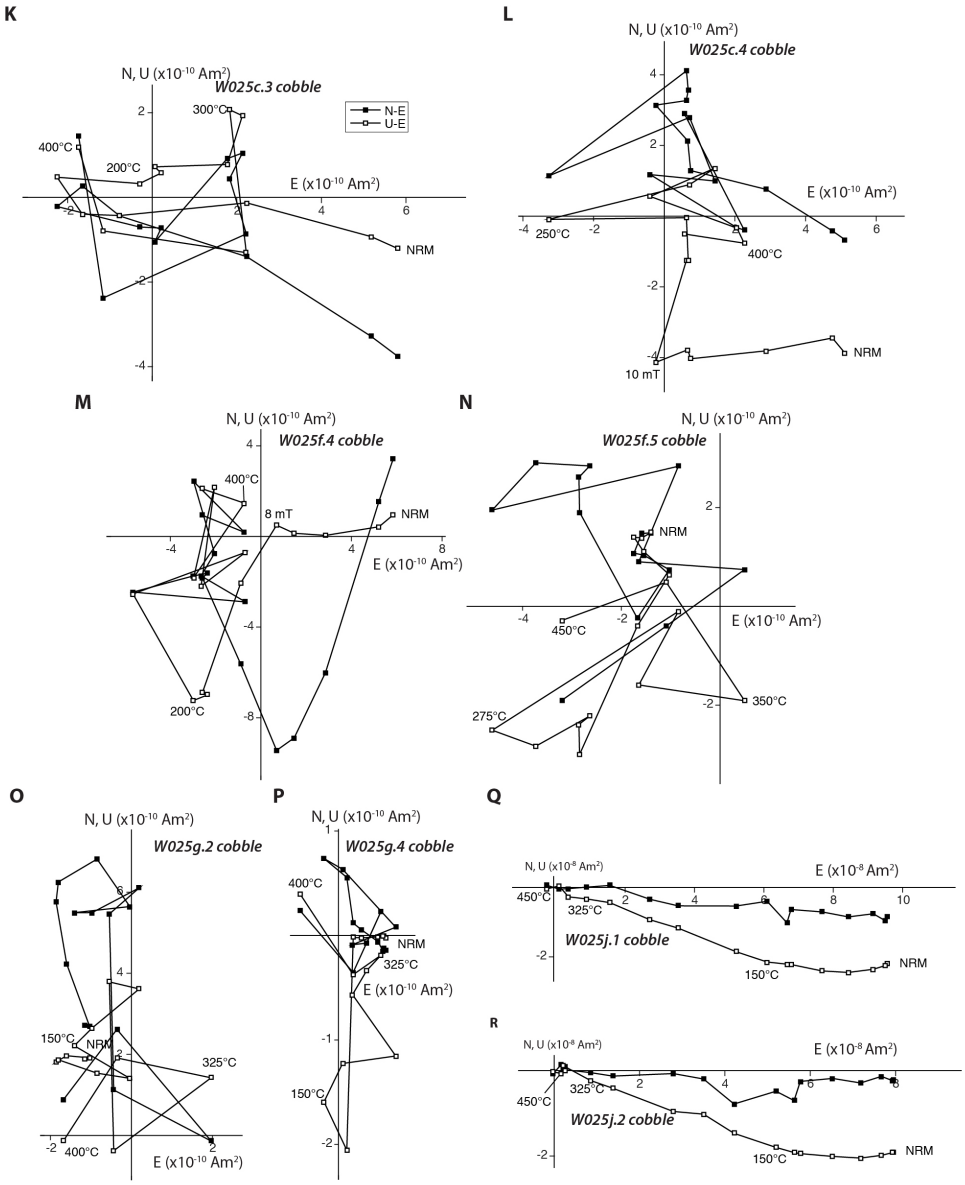

Fig. S9 continued. (K, L) Two subsamples from cobble W025c. (M, N) Two subsamples from cobble W025f. (O, P) Two subsamples from cobble W025g. (Q, R) Two subsamples from cobble W025j.

Table S1. U-Pb data for analyzed zircons from Jack Hills dolerite dyke.

	Composition					Ratios						Dates (Ma)				
Sample	Pb_c[‡]	Pb*[‡]	Th	^{206}Pb[§]	^{208}Pb[#]	^{206}Pb[††]	err	^{207}Pb[††]	err	^{207}Pb[††]	err	^{206}Pb	^{207}Pb	^{207}Pb	err	corr.
Fraction	(pg)	Pb_c	U	^{204}Pb	^{206}Pb	^{238}U	2σ%	^{235}U	2σ%	^{206}Pb	2σ%	^{238}U	^{235}U	^{206}Pb	2σ	coef.
Erawandoo Hill Dolerite Dyke (Dol6)																
z1	0.18	47	1.30	2292.5	0.393	0.182339	(.30)	1.89585	(.52)	0.07544	(.41)	1079.7	1079.6	**1079.4**	**8.3**	0.62
z2	0.24	43	0.94	2275.0	0.285	0.180479	(.10)	1.87581	(.37)	0.07541	(.34)	1069.59	1072.6	**1078.7**	**6.8**	0.48
z3	0.18	62	1.60	2857.0	0.484	0.181604	(.10)	1.88680	(.33)	0.07539	(.29)	1075.7	1076.5	**1077.9**	**5.9**	0.49
z4	0.15	44	0.94	2304.3	0.283	0.181069	(.13)	1.88130	(.39)	0.07539	(.34)	1072.8	1074.5	**1078.0**	**6.9**	0.51

Notes: Corr. coef. = correlation coefficient. Age calculations are based on the decay constants of Jaffey et al. (1971)

[†] All analyses are single zircon grains and pre-treated by the thermal annealing and acid leaching (CA-TIMS) technique. Data used in age calculations are in **bold**.

[‡] Pb_c is total common Pb in analysis. Pb* is radiogenic Pb concentration.

[§] Measured ratio corrected for spike and fractionation only.

[#] Radiogenic Pb ratio.

[††] Corrected for fractionation, spike, blank, and initial Th/U disequilibrium in magma. Mass fractionation correction of 0.25%/amu ± 0.04%/amu (atomic mass unit) was applied to single-collector Daly analyses. All common Pb is assumed to be blank. Total procedural blank was less than 0.1 pg for U. Blank isotopic composition: $^{206}Pb/^{204}Pb$ = 18.42 ± 0.35, $^{207}Pb/^{204}Pb$ =15.36 ± 0.23, $^{208}Pb/^{204}Pb$ = 37.46 ± 0.74.

Table S2. NRM components as identified by principal components analysis (PCA).

Sample	Cp.	Range	O?	δ (°)	i (°)	N	MAD/ α_{95} (°)	Notes
Dolerite:								
BCB1.1	*LT*	*10 mT-80°C*	*N*	*29.8*	*-29.6*	*3*	*3.8*	
	HT	80-440°C	*Y*	*320.1*	*-41.7*	*16*	*5.9*	*Unstable above 480°C*
BC0.1	LT	NRM-175°C	N	46.7	-63.4	8	34.6	
	HT	200-530°C	Y	30.1	23.2	17	1	
BC0.2	LT	NRM-200°C	N	259.2	-73.6	9	10.2	
	HT	225-585°C	Y	30.4	19.6	23	4.9	
BC1.1	LC	NRM-10 mT	N	235.7	-40.9	6	2.8	
	LT	10 mT-150°C	N	89.7	-50.1	6	20	
	HT	150-585°C	Y	27.2	45.4	26	2.2	
BC1.2	LC	NRM-10 mT	N	242	-38.9	6	4.7	
	LT	10 mT-150°C	N	102.4	-50	6	19.7	
	HT	150-585°C	Y	31.8	42.1	26	1.5	
Dol1.1	LC	NRM-4 mT	N	279.7	-3.2	3	1.6	
	HT	4 mT-560°C	Y	10.7	39.3	29	3.7	
Dol2.1	LC	NRM-6 mT	N	183.1	11.3	4	3.9	
	LT	10 mT-200°C	N	251.6	-76	7	14.3	
	MT 1	200-275°C	N	344.8	34	4	4.2	
	MT 2	290-360°C	N	262.8	-41.3	4	8.5	
	HT	400-560°C	Y	1.1	39.8	12	2	
Dol3.1	LC	2-10 mT	N	194.1	0.5	5	3.2	
	LT	10 mT-200°C	N	306.7	-73.9	7	16.8	
	MT 1	200-290°C	N	327.1	44.2	5	4.5	
	MT 2	290-360°C	N	238.6	-47.8	4	29.2	
	HT	440-585°C	Y	356.5	55.2	16	3.4	
Dol3.2	LC	2-10 mT	N	196.3	-1.9	*5*	8.9	
	LT	10 mT-200°C	N	210.2	-85.6	7	14.1	
	MT 1	200-275°C	N	337.3	42.4	*4*	5.7	
	MT 2	275-360°C	N	289.9	-44.8	5	20.2	
	HT	360-585°C	Y	0.8	51.2	17	2.9	
Dol5.1	LT	NRM-200°C	N	339.7	-64.6	12	16.9	
	HT	200-585°C	Y	42.2	56.5	26	2.7	
Dol5.2	LT	NRM-175°C	N	344.4	-60.1	11	29	
	HT	200-530°C	Y	41.1	53.6	17	2	
Dol6.1			*Weathered and with anomalous and self-reversing NRM*					
Dol6.2			*Weathered and with anomalous and self-reversing NRM*					
D154d.1	HT	225-585°C	Y	359.5	64.7	23	2.3	
D154d.2	HT	100-585°C	Y	0.9	65.3	28	1.4	
D154j.1			*Weathered and with anomalous and self-reversing NRM*					

D154j.2				*Weathered and with anomalous and self-reversing NRM*				
Dolerite mean	LT			28	-81.8	9	17.5	Fisher *k* = 8.6
	HT			19.3	47.5	12	10.1	Fisher *k* = 17.9
Baked quartzitic country rock:								
BCB2.1	LT	2 mT-305°C	N	321.1	-30.7	17	11.5	
	HT	320-510°C	Y	35.3	32.7	9	13.8	
BCB3.1	LT	NRM-305°C	N	291.8	-3.3	15	12.8	
	MT	305-400°C	N	245.4	17.7	4	4.2	
	HT	400-480°C	Y	36.7	20.9	5	20.7	
BCB3.2	LT	4 mT-360°C	N	296.8	5.5	18	11.8	
	HT	360-420°C	Y	347.1	66.7	3	15.5	
BCB4.1	LT	6 mT-275°C	N	342	-80.4	13	29.6	
	HT	275-360°C	Y	23.4	59.7	5	14.3	
BCB4.2	LT	8 mT-360°C	N	351.5	-29.3	16	29.8	
	HT	460-560°C	Y	63.5	44.3	8	11.9	
BCB4.3	HT	360-560°C	Y	65.8	35.9	11	8.5	
BCB4.4	HT	360-575°C	Y	59.7	52.0	15	13.8	
BCB5.1	LT	225-305°C	N	246.1	9.9	5	15.8	
	HT	320-565°C	Y	42.6	55.2	14	10.8	
BCB6.1	LT	50-360°C	N	42.4	-0.8	13	32.6	
	HT	360-500°C	Y	351.5	21.1	7	22.4	
BCB6.2	LT	290-420°C	N	87	5.2	6	17	
	HT	420-520°C	Y	39.2	51.2	7	16.6	
BCB7.1				*No stable origin-trending magnetization*				
BCB8.1	*LT*	*NRM-225°C*	*N*	*351.2*	*-55.4*	*14*	*16*	
	MT	*250-320°C*	*N*	*198*	*-11.8*	*5*	*19.9*	
	HT	*360-560°C*	*Y*	*349.4*	*-61.4*	*13*	*17.2*	*Hematite carrier; inhomogeneous with BCB8.2*
BCB8.2	LT	8 mT-200°C	N	327	-73.4	9	9.4	
	HT	275-510°C	Y	27.4	-6.8	12	30.3	
BCB9.1	*HT*	*225-320°C*	*Y*	*41.6*	*57.1*	*6*	*1.3*	*Likely lightning remagnetized*
BCB10.1	LT	4 mT-275°C	N	104.6	-21.9	14	4.9	
	HT	360-575°C	Y	92.5	-18.5	16	8.3	
BCB >3r_{dyke} mean	HT			36.5	14.1	4	65.8	Fisher *k* = 2.0; samples BCB6.1, 6.2, 8.2, and 10.1
BCB 1.2-3r_{dyke} mean	HT			44.9	50.1	7	17.7	Fisher *k* = 11.6; samples BCB3.1, 3.2, 4.1, 4.2, 4.3, 4.4, 5.1
BCB <1.2r_{dyke} mean	HT			35.3	32.7	1		Sample BCB2.1
BC3.1	LT	NRM-100°C	N	223.8	-46.7	9	5.4	
	HT	100-225°C	Y	20.1	33.5	6	14.8	
BC4.1	LC	NRM-8 mT	N	203.4	-42.1	5	4.2	
	LT	50-275°C	N	98.2	-46.1	10	22.9	

	HT	320-585°C	Y	56.5	48.7	17	10.8	
BC4.3	LT	NRM-175°C	N	197.2	-45.7	12	7.1	
	HT	225-585°C	Y	31.2	54.8	23	16.8	
BC4.4	LT	NRM-400°C	N	207.3	-32.1	21	9.2	
	HT	440-550°C	Y	35.4	60.4	9	8.4	
BC5.1	*HT*	*6 mT-560*°C	*Y*	*204.7*	*-25.1*	*29*	*2.5*	*Likely lightning remagnetized*
BC5.2	*HT*	*4 mT-560*°C	*Y*	*203.5*	*-25.6*	*30*	*2.8*	*Likely lightning remagnetized*
BC5.3	*HT*	*6 mT-575*°C	*Y*	*198.7*	*-26.8*	*32*	*1.7*	*Likely lightning remagnetized*
BC5.4	*HT*	*4 mT-565*°C	*Y*	*194*	*-30.4*	*31*	*2*	*Likely lightning remagnetized*
BC6.1	LT	6 mT-250°C	N	86.5	41.3	12	24.2	
	HT	250-500°C	Y	69.4	42.8	12	4.7	
BC7.1	LC	NRM-10 mT	N	269	-29.8	3	7.1	
	LT	10 mT-320°C	N	314.4	41.8	14	35.1	
	HT	320-570°C	Y	19.9	58.9	16	29.2	
BC7.2	LC	NRM-10 mT	N	240.9	5.7	3	8.3	
	LT	10 mT-175°C	N	353.9	-56	7	11.3	
BC8.1	LT	2 mT-360°C	N	2.5	6.6	19	23.5	
	HT	360-560°C	Y	45.1	40.6	13	7.5	
BC9.1	LT	4 mT-305°C	N	119.6	56.6	16	5.9	
	HT	305-560°C	Y	302.6	72.4	15	8.1	
BC10.1	LC	NRM-10 mT	N	250.4	59.8	3	1.6	
	HT	275-320°C	Y	263.9	33.2	4	7	
BC10.2	LC	NRM-10 mT	N	260.7	56.6	3	1.5	
	LT	10 mT-250°C	N	331.8	-62	10	9.8	
	HT	250-360°C	Y	41.7	75.5	6	15.7	
BC >3r_{dyke} mean				*334.4*	*74.2*	*4*	*49.9*	Fisher *k* = 3.0; samples BC8.1, 9.1, 10.1, 10.2
BC 1.2-3r_{dyke} mean				*44.9*	*54.5*	*5*	*13.6*	Fisher *k* = 26.3; samples BC4.1, 4.3, 4.4, 6.1, and 7.2
BC <1.2r_{dyke} mean				*20.1*	*33.5*	*1*		Sample BC3.1
D154a.1	*LC*	*NRM-10 mT*	*N*	*153.9*	*51.2*	*6*	*19.7*	
	LT	*10 mT-225*°C	*N*	*51.3*	*-9.5*	*9*	*12.2*	
	HT	*275-360*°C	*Y*	*170.2*	*-32*	*5*	*6*	*Noisy demagnetization; inhomogeneous with D154a.2*
D154a.2	*LT*	*8 mT-225*°C	*N*	*270.1*	*78.9*	*10*	*16.6*	
	MT	*225-360*°C	*N*	*45.1*	*-75.5*	*7*	*20*	
	HT	*400-570*°C	*Y*	*251*	*78.9*	*12*	*28.4*	*Noisy demagnetization; inhomogeneous with D154a.1*
D154b.1	*LC*	*NRM-6 mT*	*N*	*160.9*	*-5.6*	*4*	*18.8*	
	HT	*6 mT-290*°C	*Y*	*31.4*	*-66.1*	*14*	*9.9*	*Noisy demagnetization*
D154c.1	LC	NRM-10 mT	N	117	3.7	6	31.9	
	LT	50-250°C	N	247.4	9	9	25.9	
	HT	250-290°C	Y	29	11.1	3	10.9	
D154c.2	LC	NRM-6 mT	N	187.3	-39.8	4	11.2	
	HT	6 mT-150°C	Y	66.8	6.9	8	5.2	
D154c.3	LC	NRM-10 mT	N	182	-19	6	15.4	
	LT	50-400°C	N	46.5	-62.3	14	18.9	

	HT	400-500°C	Y	53.7	65.6	5	11.7	
D154e.1	HT	290-565°C	Y	21.2	50.9	17	6.1	
D154e.2	LT	10 mT-440°C	N	311	-32.2	18	24.5	
	HT	440-540°C	Y	26.6	58.9	8	7.1	
D154f.1	LT	NRM-200°C	N	2.9	-58.4	13	3.8	
	HT	320-520°C	Y	29.3	51	10	5.9	
D154g.1	LT	50-360°C	N	37.8	-43.8	14	16.2	
	HT	360-560°C	Y	83.1	51.7	13	20.3	
D154h.1	LT	10 mT-80°C	N	354	-59.5	3	4.7	
	HT	80-200°C	Y	104.1	73.6	5	10.6	Not clearly origin-trending
D154h.2	LT	10 mT-80°C	N	356.5	-59.5	3	3.7	
	HT	150-225°C	Y	80.2	-7.5	4	6.2	
D154i.1	LT	10 mT-275°C	N	339.3	-33.9	11	18.4	
	HT	275-320°C	Y	78	30.1	4	7.7	
D154i.2	LT	10 mT-150°C	N	0.1	-46.4	6	3.1	
	MT	150-275°C	N	117.3	13.9	6	34.7	
	HT	275-305°C	Y	355.7	22.4	3	6.2	
D154i.3	LT	10 mT-80°C	N	355	-39.8	3	3.8	
	HT	150-290°C	Y	44.5	48.5	7	5.4	
D154i.4	LT	10 mT-250°C	N	358.6	-47.2	10	14.9	
	HT	250-305°C	Y	335.2	55.6	4	3.5	
D154 >3r_{dyke} mean	HT			48.5	48.8	8	28.1	Samples D154f, g, h, i; Fisher *k* = 3.9
D154 1.2-3r_{dyke} mean	HT			40.6	40.4	5	31.9	Samples D154c, e; Fisher *k* = 5.4
BC, BCB, and D154 quartzite mean	LT			350.3	-50.7	33	27.6	Fisher *k* = 1.8
Monzogranite:								
D182a.1	LC	NRM-8 mT	N	113.6	22.7	5	14.9	
	HT	10 mT-290°C	Y	342.2	59.4	12	10.4	
D183.1	LT	10 mT-150°C	N	339.9	-50	6	1.3	
	HT	360-560°C	Y	337.2	45.1	13	18.5	
D183.2	LT	10 mT-150°C	N	357.8	-54.7	6	2.4	Using second 150°C step
	HT	150-290°C	Y	340.6	9.6	9	7.2	Using second 150°C step
D184.1	LT	10 mT-150°C	N	355	-57.8	6	4.5	Using second 150°C step
	HT	*150-575°C*	*Y*	*57.9**	*29**	*25*	*25.1*	*Circle fit; hematite carrier; Using second 150°C step*
D185.1	LT	10 mT-80°C	N	19.7	-45.4	3	4.5	
	HT	80-360°C	Y	329.9	72.7	13	10.6	
D185.2	LT	10 mT-80°C	N	341.3	-60.3	3	2.9	
	HT	225-480°C	Y	5.7	55.5	12	10.4	
D186.1	LT	6 mT-225°C	N	354.1	-46.2	10	0.9	
	HT	290-540°C	Y	351.9	4.2	14	10.3	
D187.1	LC	2-10 mT	N	317.4	-17.8	5	5.8	
	LT	10 mT-225°C	N	27.2	-54.5	8	7.4	
	HT	225-500°C	Y	359	28.5	14	8.5	
D187.2	LT	4 mT-200°C	N	355.2	-55.7	10	4.6	

	HT	200-540°C	Y	341.6	19.9	18	7.9	
D187.3	LC	NRM-10 mT	N	344.2	-9.5	6	8.9	
	LT	10 mT-275°C	N	348.7	-60.8	10	3.3	
	HT	275-570°C	Y	0.1	35.4	18	5.6	
D187.4	LT	6 mT-200°C	N	358	-62.7	9	4.6	
	HT	200-540°C	Y	353.9	32.2	18	4.9	
D188.1	*LT*	*10 mT-80°C*	*N*	*134.0*	*-52.3*	*2*		*Low thermal stability, 2 point fit*
	HT	80-305°C	Y	34.8	68.4	11	5	
D188.2	*LT*	*10 mT-80°C*	*N*	*125.7*	*-57.9*	*2*		*Low thermal stability, 2 point fit*
	HT	100-320°C	Y	0.4	69.5	11	5.8	
D189.1	*HT*	*6 mT-585°C*	*Y*	*318*	*-22.5*	*32*	*2.3*	*Likely lightning remagnetized*
D189.2	*HT*	*4 mT-585°C*	*Y*	*313.3*	*-22.2*	*33*	*3.5*	*Likely lightning remagnetized*
Blob4a.1	LT	NRM-200°C	N	356.8	-37.6	12	11	
	HT	200-520°C	Y	302.4	80.1	16	29.1	
Blob4a.2	LT	4 mT-175°C	N	357.8	-40.2	9	11.2	
	HT	175-520°C	Y	30.3	82.1	16	20	
Blob4a.3	LT	4 mT-275°C	N	335.4	-36.3	13	6.6	
	HT	290-510°C	Y	70.1	64.8	11	22.3	
Blob4a.4	LT	4 mT-275°C	N	349.1	-45.4	14	13.1	Using second 100°C step
	MT	275-520°C	N	43.6	36.7	14	21.6	No origin-trending HT component
Blob5b.1	LC	2-10 mT	N	179.5	-18.1	5	4.3	
	HT	100-440°C	Y	16.6	39	15	9.4	
Blob5b.2	LC	2-10 mT	N	178	-19.8	5	5.6	
	LT	*10 mT-250°C*	*N*	*327.9*	*-12.9*	*9*	*22*	*Using third 80°C step*
	HT	250-520°C	Y	16	72.3	14	11.2	
Blob5c.1	LT	2 mT-200°C	N	10.2	-53.1	11	4.8	
	HT	200-520°C	Y	357.2	64.5	16	6.7	Using first 520°C step
Blob5c.2	LT	8 mT-100°C	N	4.5	-53.5	4	1.6	
	HT	*125-150°C*	*Y*	*354.4*	*60.2*	*2*	*12.1*	*Very weak moment by 125°C*
Blob5c.3	LT	2 mT-80°C	N	6.8	-54.7	6	4.2	
	HT	150-510°C	Y	17.3	42.3	15	5.5	
Monzogranite mean	LT			357.2	-51.9	17	5.2	Fisher k = 48.3
	HT			358	51.9	19	11.7	Fisher k = 9.2

Quartzitic country rock:

D145.1	LT	2 mT-305°C	N	42.9	-44.6	17	5.2	
	HT	*305-420°C*	*Y*	*341.5*	*-55.5*	*5*	*7.3*	*Hematite carrier; present field direction*
D145.2	LT	4 mT-275°C	N	50.5	-49.3	14	9.4	
	HT	*275-400°C*	*Y*	*351.6*	*-39.2*	*6*	*5.4*	*Hematite carrier; present field direction*
D145.3	LT	2 mT-80°C	N	41.6	-53.9	7	4.6	
	HT	*80-360°C*	*Y*	*4.4*	*-49.2*	*13*	*4.7*	*Hematite carrier; present field direction*
D145.4	LT	4 mT-320°C	N	33.1	-55.6	17	7.1	

	HT	*320-520°C*	*Y*	*337.1*	*-43.5*	*10*	*9.6*	*Hematite carrier; present field direction*
D192b.1	LC	NRM-6 mT	N	338.6	6.1	3	3.9	*Noisy demagnetization*
	LT	*6 mT-250°C*	*N*	*136.9*	*-1.6*	*11*	*30.6*	
	HT	250-320°C	Y	15.4	38.7	5	36	
D192b.2	LC	NRM-6 mT	N	312.9	-10.4	4	33.5	
	LT	6 mT-225°C	N	74.7	-29.4	10	16.9	
	HT	225-360°C	Y	343.7	77.9	7	19.2	
D194b.1	LT	NRM-225°C	N	116.6	35.5	12	32.9	No origin-trending HT component
D194b.2	LT	150-225°C	N	310.5	57.3	4	18	No origin-trending HT component
D194b.3	LC	NRM-10 mT	N	193.1	-17.8	6	19.4	
	HT	275-290	Y	63.1	61	2	1.1	
D194c.1	LC	2-10 mT	N	45.3	22.4	5	24.9	No origin-trending component
D194c.2	LC	2-10 mT	N	72.4	3.1	5	34.2	
	LT	80-250°C	N	351.2	-64.2	8	21.4	
	HT	290-510°C	Y	357.4	62	10	11.5	
D194c.3	LC	2-10 mT	N	41.3	-14.2	5	31.3	
	LT	100-360°C	N	64.1	-17.9	12	15.9	
	HT	400-520°C	Y	17.4	72.3	8	13.2	
D195a.1	HT	225-360°C	Y	3.8	61	7	0.7	
D195a.2	HT	275-360°C	Y	4.4	61.7	5	0.7	
D195a.3	HT	290-360°C	Y	2.5	62	4	0.8	
D195b.1	LT	NRM-125°C	N	328	-67	9	11.5	
	HT	225-320°C	Y	1.6	52	6	3.7	
D195b.2	HT	200-320°C	Y	0.1	50.3	7	4.3	
Quartzite mean	LT			46.2	-41.8	10	38.1	Fisher k = 2.3
Quartzite mean	HT			9.3	61.2	10	8.8	Fisher k = 27.7

Fold Tests:

D102:								
D102a.1	LT	NRM-200°C	N	52.6 79	1.4 27.6	9	16.6	
	HT	200-325°C	Y	59.9 28	-49.3 9.5	5	2.9	
D102b.1	LT	NRM-200°C	N	167.6 138.9	50.8 1.5	9	8.7	
	HT	275-350°C	Y	354.8 66.8	55.3 29	3	1.8	
D102b.2	LT	NRM-200°C	N	204.4 130.7	65.9 24.2	9	13.7	
	HT	275-350°C	Y	350.3 71.2	59 31.2	4	1.9	
D102b mean	HT			352.7 69	57.2 30.1	2		
D102c.1	LT	4 mT-200°C	N	41.6 13.3	-19.7 -12.9	7	6.5	

D102c.3	LT	4 mT-150°C	N	46.2 8.3	-24.8 -17.4	6	12.9	
D102d.1	LC	NRM-10 mT	N	281.5 276.1	43.1 -33	6	9.6	
	LT	200-325°C	N	10.2 53.4	-75.3 4.3	5	4.1	
	MT	325-400°C	N	320.4 319.3	14.7 -13.4	3	1.4	
	HT	400-662°C	Y	115.7 89.7	-59.1 15.5	17	26.6	
D102d.3	LT	150-325°C	N	347.1 30.6	-54.3 3.4	6	8.8	
	MT	325-400°C	N	285.4 36.7	-50.8 -32.6	3	11	Using second 275°C step
	HT	400-475°C	Y	38.7 331.3	5.5 63.2	3	22	
D102d mean	HT			62.9 61.8	-32 53.8	2		
D102e.1	LT	4 mT-275°C	N	145.4 264.3	-35 -48.6	9	10.3	
	HT	275-350°C	Y	183 267.5	-56.6 -15.4	4	12	
D102e.3	LT	4 mT-200°C	N	108 314.5	-34 -56.5	7	9	
	HT	250-325°C	Y	190.4 248.3	-38.8 -15.3	4	9.7	
D102e mean	HT			187.3 257.9	-47.8 -15.6	2		
D102f.1	LT	NRM-200°C	N	87.2 94.6	12.7 -2.7	9	3	
	HT	200-325°C	Y	108.9 123.9	36.1 -11.9	5	3.5	
D102 HT mean				80.5 66.8	-17 28.9	5	118.7 117.2	Fisher k_{geo} = 1.1 Fisher k_{tilt} = 1.1
D197:								
D197a.1	LT	NRM-100°C	N	41.5 92.6	-45.9 -27.9	7	17	
	MT	100-350°C	N	330.7 6.6	-21.6 -81.5	9	13.4	
	HT	350-640°C	Y	346.7 50	-24.6 -69.9	17	0.8	
D197b1.1	LT	4 mT-300°C	N	102.1 19.6	47.7 67	9	27.6	
	MT	300-325°C	N	4.9 350.4	39.9 4.3	2		2 point fit
	HT	350-640°C	Y	340.3 78.4	-50.8 -69.7	17	13.4	
D197b2.1	MT	250-325°C	N	351 313.3	40 45	4	4.3	
	HT	325-640°C	Y	157.2 192.9	55.3 34.4	18	2.4	

D197c.1	LT	NRM-250°C	N	85.8 85.9	-15.6 15.3	10	20.1	
	MT	250-325°C	N	342.1 339.6	43.5 -21.6	4	2.8	Origin-trending; Labeled MT because similar temperature range to MT components of other samples; Using second 275°C step
D197d.1	LT	NRM-100°C	N	84.3 92.3	-66.5 -36.2	7	18.5	
	MT	100-325°C	N	354 358.5	-4.6 -11.8	7	10.8	
	HT	350-640°C	Y	70 88.4	-73.7 -44.2	17	2.4	
D197d.2	LT	NRM-100°C	N	154.1 132.6	-55.1 -31.9	7	14.2	
	MT	100-350°C	N	334.1 337.3	1.9 -15.7	8	6.4	Using first 275°C step
	HT	350-640°C	Y	72 91	-77.6 -47.7	17	4.6	
D197d mean	MT			344 348	-1.4 -14	2		
	HT			70.9 89.7	-75.7 -45.9	2	8.6	
D197 mean	MT			345.8 340.9	21 -12.7	5	32 49.5	Fisher k_{geo} = 5.4 Fisher k_{tilt} = 2.5
D197 mean	HT			1.8 114.6	-52.2 -58.9	4	90 92.6	Fisher k_{geo} = 1.0 Fisher k_{tilt} = 1.4
Erawandoo Hill pebble conglomerates (clast and matrix samples):								
EHJH5:								
0h	LT	NRM-200°C	N	74.8	-83.2	4	8.8	Clast
	HT	250-325°C	Y	334	11.6	4	11.2	
0i	LT	150-275°C	N	59.1	17.5	4	19	Clast
	HT	275-335°C	Y	339.2	19	4	3.5	
0j	LT	NRM-250°C	N	36	1.1	5	13.9	Clast
	HT	300-335°C	Y	333.4	14.4	3	5.1	
0k	LT	NRM-250°C	N	155.5	44.7	5	19.4	Clast
	HT	275-335°C	Y	351.5	-21.6	4	18.4	
2aa	HT	275-335°C	Y	318.8	-4.4	4	2.7	Clast
2ab	LT	NRM-250°C	N	235.2	-75.8	5	18.4	Clast
	HT	275-325°C	Y	319.7	30	3	4.6	
2c	LT	NRM-250°C	N	63.5	-12.9	5	8.5	Clast
	HT	300-325°C	Y	338.7	-7.6	2	9.4	
2e	HT	250-335°C	Y	345.2	31.4	5	3.2	Clast
2f	LT	NRM-250°C	N	35.9	-38.2	5	13.7	Clast
	HT	300-335°C	Y	350.4	39.3	3	3.3	
2j	LT	NRM-275°C	N	329	-17.5	6	12.2	Clast
	HT	275-345°C	Y	323.1	35.8	5	13	
2l	LT	NRM-200°C	N	130.2	-8.5	4	5.2	Clast
	HT	250-325°C	Y	326.9	-3.7	4	8.4	

3f	HT	75-395°C	Y	337.6	34.8	14	5.6	Clast
3g	HT	250-335°C	Y	334.2	6.3	5	6.9	Clast
3j	HT	300-345°C	Y	312.5	9.2	4	14.2	Clast
3k	LT	150-275°C	N	333.5	-19.5	4	8.6	Clast
	HT	275-335°C	Y	326.2	51.6	4	5	
3m	HT	250-335°C	Y	343.8	21.9	6	3.8	Clast
4a	HT	200-325°C	Y	321.5	24	5	10.1	Clast
4e	HT	200-335°C	Y	328	9	6	5.2	Clast
4f	HT	250-335°C	Y	331.6	25.3	5	4.4	Clast
4h	LT	NRM-275°C	N	340.3	-35.1	6	7.4	Clast
	HT	275-335°C	Y	324.4	5.8	4	5.1	
4i	LT	NRM-150°C	N	334.5	-52.5	3	0.8	Clast
	HT	150-325°C	Y	303.4	-22.4	6	19.2	Noisy demagnetization
4k	HT	250-335°C	Y	326.1	1.6	5	1.7	Clast
4l	HT	250-355°C	Y	328.5	-5.1	7	1.7	Clast
4m.1	LT	NRM-200°C	N	104	1.2	4	32.4	Clast
	MT	200-325°C	N	227.7	0.5	5	23.7	
	HT	325°C	Y	353.6	15.5	1		Single point plus origin
4m.2	LT	NRM-200°C	N	297.6	16.4	4	1.4	
	HT	200-300°C	Y	330.9	1.2	4	13	Clast
4m clast mean	HT			342	8.5	2	61.5	
5c	LT	150-275°C	N	309.1	-36.6	4	10.4	Clast
	HT	300-335°C	Y	334	22.8	3	2.6	
5e	LT	150-250°C	N	41.7	-5.5	3	17.6	Clast
	HT	275-325°C	Y	337.1	16.1	3	2.6	
5f	LT	NRM-150°C	N	344.3	-57.3	3	0.9	Clast
	HT	200-325°C	Y	30.3	28.7	5	5.5	
5g.1	LT	250-300°C	N	310.3	25.1	3	8.3	Clast
	HT	300-325°C	Y	314.7	-41.3	2	4.8	
5g.2	HT	250-325°C	Y	321.2	23.6	4	6	Clast
5g clast mean	HT			318.3	-8.9	2	90	
5h	LT	NRM-200°C	N	27.9	52.4	4	3.5	Clast
	HT	250-325°C	Y	325.1	1.9	4	4.5	
5i	LT	NRM-200°C	N	242	-47.4	4	7.8	Clast
	HT	275-300°C	Y	338	-17.1	2	4.3	
5j				No stable magnetization (clast)				
s1f	LT	NRM-200°C	N	335.5	-54.4	4	2.7	Matrix
	MT	200-325°C	N	21.1	2.5	5	3.4	
	HT	325-625°C	Y	5.5	-29.3	14	16	
s1h	LT	250-335°C	N	355.5	8.9	5	3.9	Matrix
	HT	335-625°C	Y	38.4	1.3	13	2.4	Not fully demagnetized
s2b	LT	NRM-150°C	N	325.8	-24	3	2.6	Matrix
	HT	275-625°C	Y	359	-5.4	15	6.7	Not fully demagnetized
s2k.1	LT	NRM-325°C	N	19.7	19.6	8	7.1	Matrix
	HT	325-625°C	Y	37.6	8	13	6.1	Not fully demagnetized
s2k.2	LT	NRM-150°C	N	201.1	-29.7	3	1.6	Matrix
	MT	150-345°C	N	20.5	24.3	8	6.4	

	HT	345-660°C	Y	38.1	7.4	13	6.5	
s3a	LT	NRM-150°C	N	352.1	-37.1	3	2.3	Matrix
	MT	150-335°C	N	334	47.2	7	8.9	
	HT	335-660°C	Y	32.7	35.8	14	5.1	
s3g	MT	150-335°C	Y	352.7	27.8	7	5.9	Matrix
EHJH5 clast/matrix mean	LT			1.9	-33.4	26	31.6	Fisher k = 1.8
EHJH5 clast mean	HT			332.3	12.3	30	7.9	Fisher k = 12.2, R = 27.6
EHJH6:								
a2m	LT	50-175°C	N	215.4	10.8	4	6.5	Matrix
	HT	175-335°C	Y	265	55.2	14	11.7	
a3m	No stable magnetization (matrix)							
a4m	HT	50-200°C	Y	334.7	60.6	5	1.7	Matrix
a5m	LT	NRM-150°C	N	209.8	3.7	4	20.1	Matrix
	HT	150-200°C	Y	35.9	47.3	3	8.2	
a6m	LT	100-175°C	N	268.5	43.4	3	10.2	Matrix
	HT	175-335°C	Y	0.3	72.3	13	31.2	
a7m	LT	50-150°C	N	236.8	3.2	3	17.5	Matrix; No origin-trending HT component
a8c	No stable magnetization (clast)							
a9c	LT	NRM-150°C	N	135.3	21.7	4	9.4	Clast
	HT	*150-275°C*	*Y*	*164.8*	*16.3*	*9*	*28.2*	*Ambiguous fit*
a10c	LT	50-150°C	N	270.3	0	3	4.7	Clast
	HT	150-225°C	Y	359.5	48.1	4	9.7	
a11c	LT	NRM-175°C	N	204	38.9	5	16.1	Clast
	HT	225-275°C	Y	17	40.3	6	6.2	
a12c	LT	50-200°C	N	281.6	-25.9	5	13.7	Clast
	MT	200-255°C	N	78.7	25.1	5	27.3	Ambiguous fit; no origin-trending HT component
a13c	HT	175-325°C	Y	283.2	63	13	9	
a15ac	LT	NRM-235°C	N	244	-32.2	8	7.6	Clast
	MT	255-315°C	N	100.6	48.1	8	10.1	No origin-trending HT
a15bc	LT	NRM-235°C	N	136.4	-64	8	39.9	Clast
	MT	265-285°C	N	303	38.4	3	3.6	
	HT	285-335°C	Y	10.5	49	6	10.5	
a16c	LT	100-265°C	N	238.5	-39.7	9	13.1	Clast
	HT	265-335°C	Y	246.7	17.4	8	5.4	
a17c	LT	NRM-265°C	N	181.8	-45.1	11	16.2	Clast
	HT	265-335°C	Y	236.7	6.6	8	1.9	
a18c	LT	NRM-305°C	N	200.6	-34.6	15	25	Clast
	HT	305-345°C	Y	23.6	48.6	5	2.8	
c01c	LT	50-175°C	N	309.6	3.7	4	4.3	Clast

	HT	*175-335°C*	*Y*	*196.4*	*-54.5*	*12*	*13*	*Not completely demagnetized*
c02c	LT	100-225°C	N	265.8	-4.5	5	18.4	Clast; ambiguous fit; weak moment; no origin-trending HT component
c03c	LT	50-200°C	N	125.7	-4.6	5	9.6	Clast; no origin-trending HT
c04m	LT	NRM-100°C	N	45.5	-54.4	3	19.9	Matrix; ambiguous fit
	HT	100-250°C	Y	253.2	61.1	6	13.8	
c05c.1	LT	NRM-225°C	N	235.2	18.1	7	11.5	Clast; no origin-trending HT component
c05c.2	LT	NRM-175°C	N	91.1	33.5	5	37.4	Clast; Ambiguous fit; no origin-trending HT component
c05c.3	LT	100-175°C	N	296.6	35.8	3	10	Clast; no origin-trending HT component
c05c.4	LT	NRM-100°C	N	349	16.9	3	1.7	Clast
	MT	150-200°C	N	23.5	-43.7	3	3	
c07m	LT	150-200°C	N	20.7	48.9	3	2.3	Matrix
	HT	200-225°C	Y	4.4	66.1	2	6.9	Two point fit
c08c	No stable magnetization (clast)							
c09m	LT	50-175°C	N	322.5	59.8	4	8.5	Matrix
	HT	200-335°C	Y	211.6	60.7	11	5.3	Not fully demagnetized
c10c	LT	NRM-200°C	N	270.8	-33	6	36.3	Clast; ambiguous fit
	HT	200-225°C	Y	46.7	49.4	2	2.6	Two point fit
c11c.1	LT	NRM-150°C	N	320.9	-1.7	4	2.9	Clast; no origin-trending HT component
c11c.2	LT	175-200°C	N	179.8	-58.3	2		Clast; two point fit; no origin-trending HT component
c11c.3	LT	NRM-200°C	N	304.4	-6	6	11.7	Clast; no origin-trending HT component
c11c.4	LT	100-200°C	N	245.3	64.5	4	11.4	Clast; ambiguous fit; no origin-trending HT component
c11c.5	LT	NRM-200°C	N	148.9	54.7	6	5.1	Clast
	MT	200-350°C	Y	262.7	-66.1	12	36	Ambiguous fit; no origin-trending HT component
c12m	LT	NRM-225°C	N	124.9	0.6	7	14.9	Matrix
	HT	225-335°C	Y	245.3	37.1	10	2.7	
c13m	LT	100-285°C	N	217	-5.3	9	15.2	Clast
	HT	285-335°C	Y	21.2	50.1	6	2.7	Matrix
c14m	HT	305-335°C	Y	358.5	52.9	4	5.4	Matrix
c15m	HT	200-325°C	Y	239.5	25.6	10	1.4	Matrix
c16c	HT	100-265°C	Y	229.9	23.3	7	2.8	Clast
c20m	LT	NRM-100°C	N	26.3	-57.2	3	5.3	Matrix
	HT	100-200°C	Y	121.2	29.5	4	7.8	
c21c	HT	100-200°C	Y	336.5	56.7	4	3.4	Clast
c22c.1	No stable magnetization (clast)							
c22c.2	No stable magnetization (clast)							
c24m	LT	150-225°C	N	2.4	59	4	8.2	Matrix
	HT	*225-500°C*	*Y*	*202.4*	*42.5*	*14*	*5.7*	*Not fully demagnetized*

c26m	LT	50-175°C	N	257.5	0.4	4	28.2	Matrix
	HT	*175-500°C*	*N*	*219.2*	*51.7*	*16*	*13.9*	*Not fully demagnetized*
EHJH6 clast/matrix mean	LT			244.7	8.7	34	34.3	Fisher *k* = 1.5
EHJH6 clast/matrix mean	HT			312	72.5	22	19	Fisher *k* = 3.5
EHJH7:								
a01m	LT	NRM-150°C	N	313.2	-11.5	4	8.1	Matrix
	MT	150-250°C	N	49.5	85.3	4	11.9	
	HT	250-350°C	Y	315.4	-6.4	10	23.5	Ambiguous
a02m	LT	NRM-150°C	N	318.6	-2.6	4	6.2	Matrix
	HT	150-500°C	Y	289	16.3	17	19.1	Not fully demagnetized
a03m	LT	100-225°C	N	355.7	28.2	5	19.9	Matrix
	HT	225-450°C	Y	334.4	-16.9	13	26.4	
a04c	LT	NRM-150°C	N	325.8	19.9	4	7.2	Clast
a05m				No stable magnetization (matrix)				
a06m	LT	100-265°C	N	328.5	36	7	12.5	Matrix
	HT	275-335°C	Y	333	13.4	7	22.7	
a07m	LT	150-250°C	N	323.6	9.3	5	6.9	Matrix
	HT	250-325°C	Y	41.1	0.1	8	23.9	
a08c.1	LT	150-250°C	N	340.5	-18.7	5	5	Clast
	HT	250-400°C	Y	355.5	-23.1	11	17.3	Not fully demagnetized
a08c.2	LT	200-250°C	N	355.4	-45.1	3	1.2	Clast
	HT	250-450°C	Y	335.7	-18	13	12.8	
a08c.3	LT	175-225°C	N	347.6	-16.1	4	10.9	Clast
	HT	315-500°C	Y	343.3	-10.4	7	7.3	Not fully demagnetized
a08c clast mean	HT			344.7	-17.3	3	17.5	Mean of subsamples 1, 2, and 3
a09c.1	LT	NRM-315°C	N	26	-2.7	14	7.8	Clast
	MT	315-335°C	N	51.6	69.1	3	8	
	HT	335-500°C	Y	19.4	-5.7	5	7.6	
a09c.2	HT	250-325°C	Y	341.2	-3	8	3.6	
a09c.3				No stable magnetization (clast)				
a09c clast mean	HT			0.3	-4.6		74.1	Mean of subsamples 1 and 2
EHJH7 clast/matrix mean	LT			338.7	-0.2	10	20.1	Fisher *k* = 5.7
EHJH7 clast/matrix mean	HT			342.6	-6.2	10	21.1	Fisher *k* = 5.6
Cobble conglomerates (all samples are from clasts):								
D107c.2	LC	NRM-6 mT	N	237.8	-51.8	4	10.3	
	MT	150-325°C	N	89.4	-13.3	6	15.3	
	HT	325-662°C	Y	34.5	-65.3	17	21.7	Hematite carrier
D107c.3	LT	NRM-200°C	N	137.8	-81.7	9	5.6	
	MT	275-350°C	N	100.1	-28.7	4	6	

	HT	350-600°C	Y	18.1	-57	13	21	Hematite carrier
D107c clast mean	MT			94.5	-21.1	2	41	Mean of subsamples 2 and 3
D107c clast mean	HT			25.2	-61.4	2	25.1	
D107g.1	LT	NRM-100°C	N	202	-3.4	7	7.1	
	HT	100-560°C	Y	174.7	21	17	5.3	
D107h.1	LT	4 mT-275°C	N	216.3	53.6	9	11.9	
	HT	275-325°C	Y	143.8	55.8	3	4.7	
D107i.1	LT	6 mT-275°C	N	206.2	52	8	3.9	
	HT	275-325°C	Y	182.8	67.5	3	3.3	Not clearly origin-trending
D108.1	LT	4 mT-275°C	N	265.9	8.9	9	11.1	
	HT	275-325°C	Y	236.1	6	4	6.4	
D108.2	LT	4 mT-275°C	N	271.5	-3.1	9	15.7	
	HT	275-325°C	Y	251.6	-10.3	3	4.1	
D108 clast mean	HT			243.8	-2.2	2		Mean of subsamples 1 and 2
D109a.1	LT	2-10 mT	N	255	57.3	5	6.6	
	HT	150-565°C	Y	216.8	-43.5	18	2.6	
D109b.1	HT	4 mT-325°C	Y	108	-48.5	11	1.5	
D109b.2	HT	4 mT-570°C	Y	105.2	-46.6	25	2.1	Suspect HT component: low minimum blocking temperature
D109b clast mean	HT			106.6	-47.5	2		Mean of subsamples 1 and 2
D110.1	LT	4 mT-250°C	N	268.4	-48.2	8	12.4	
	HT	275-300°C	Y	276.5	-43.5	2	3.1	
D111c.45				No stable magnetization				
D111c.6				No stable magnetization				
D111d.2	LC	6-10 mT	N	221.5	13.4	3	3.5	
	LT	10 mT-250°C	N	12	48.3	5	19.3	
	MT	250-325°C	N	48.9	-22.3	4	6.6	No origin-trending HT component
D111d.3	LT	NRM-150°C	N	192.1	-48.5	8	21.5	
	MT	150-250°C	N	110.9	-23.5	3	12.5	No origin-trending HT component
D111e.2	LC	NRM-10 mT	N	152.2	10.5	6	12.4	
	LT	10 mT-300°C	N	44.4	36.3	7	15.2	No origin-trending HT component
D111e.3	LT	6 mT-200°C	N	59.8	45.8	6	20.6	
	MT	200-250°C	N	112.8	-70.7	2		2 point fit; No origin-trending HT component
D111h.1	LC	NRM-6 mT	N	304.8	-37.8	4	11.9	No origin-trending HT component
D111h.2	LC	2-8 mT	N	260.4	-30.3	4	19.7	
	LT	8 mT-275°C	N	107.9	4.1	7	30.5	No origin-trending HT component
D111i.5	LT	NRM-150°C	N	74.6	40	8	35.1	No origin-trending HT component
D111i.6	LT	6 mT-250°C	N	2	-12.8	7	15.9	
	HT	275-325°C	Y	214.1	4.8	3	13	Inhomog. with subsample 5
D111j.1	LT	NRM-250°C	N	97.8	-41	10	15.2	No origin-trending HT component
D111j.2	LT	NRM-200°C	N	96.7	13.1	9	13.6	
	MT	200-300°C	N	41	-1.1	4	30.4	No origin-trending HT component
D112c.1	LT	8 mT-275°C	N	84.8	16.1	7	17.4	No origin-trending HT component
D112c.2	LC	2-6 mT	N	164.7	-43.1	3	7.3	

	LT	6 mT-200°C	N	100.9	-8.7	6	21.5	No origin-trending HT component
D112d.1	LT	8 mT-275°C	N	293.6	6.9	7	26.1	No origin-trending HT component
D112d.3	LC	NRM-6 mT	N	262.2	-28.1	4	3.7	
	LT	6 mT-250°C	N	266.6	39	7	11.3	No origin-trending HT component
D112e.2	LT	8 mT-250°C	N	115.5	-26.7	6	18.1	
	MT	250-300°C	N	16.9	39.7	3	8.2	No origin-trending HT component
D112f.1	LC	NRM-4 mT	N	261.5	-32.8	3	14.4	
	LT	4 mT-275°C	N	94.4	-37	9	21.1	
	HT	275-325°C	Y	231.9	1.6	3	12.6	Not clearly origin-trending
D112g.1	LC	NRM-10 mT	N	186.8	-1.2	6	15.7	
	LT	100-250°C	N	34.6	59.5	4	33.4	Ambiguous; no origin-trending
D112g.2	LC	2-10 mT	N	71.8	72.4	5	32.8	
	LT	200-275°C	N	71	-16.6	3	29.6	
	MT	275-350°C	N	260.4	-8	4	19.2	No origin-trending HT component
D112j.2	LT	NRM-150°C	N	253.8	-62.6	8	20.1	
	MT	150-275°C	N	234.5	69.9	4	13.4	No origin-trending HT component
D112j.3	LT	8 mT-200°C	N	240.2	15.4	5	40	
	MT	200-275°C	N	75.8	38.9	3	19.9	No origin-trending HT component
D112k.3	LT	250-325°C	N	148.6	65.2	4	9.8	No origin-trending HT component
D112k.4	LT	150-250°C	N	166.6	32.3	3	8.5	No origin-trending HT component
D112l.1	LC	2-10 mT	N	205.4	69.3	5	16.9	No origin-trending HT component
D112l.2	LT	8 mT-275°C	N	112.8	19	7	33.3	No origin-trending HT component
D192c.1					No stable magnetization			
W025a.2	LT	NRM-250°C	N	84.2	-44.9	10	14.2	No origin-trending HT component
W025a.3	LC	NRM-10 mT	N	93.6	-33.3	6	29.2	No origin-trending HT component
W025b.1	LT	NRM-150°C	N	46.7	-1.7	8	4.4	No origin-trending HT component
W025b.3	LT	NRM-150°C	N	4.1	-46.8	8	6.3	No origin-trending HT component
W025c.3	LC	NRM-10 mT	N	115.3	7.1	6	6.7	
	LT	10 mT-250°C	N	253.5	4.6	5	24.7	No origin-trending HT component
W025c.4	LC	NRM-10 mT	N	122.4	-3.5	6	8.1	
	LT	10 mT-200°C	N	229.8	72.7	4	9.4	No origin-trending HT component
W025d.f1	LT	NRM-150°C	N	184.4	-73.6	8	3.6	No origin-trending HT component
W025f.4	LC	NRM-8 mT	N	20.5	-2.1	5	3.6	
	MT	8 mT-200°C	N	156.5	-43.3	5	4.7	No origin-trending HT component
W025f.5	LC	NRM-10 mT	N	1.1	-48.7	6	16.2	
	LT	10 mT-250°C	N	152.3	-34.1	5	17.2	
	MT	275-350°C	N	276.7	14.1	4	29.9	No origin-trending HT component
W025g.2	LC	NRM-8 mT	N	167.6	-1	5	3.7	
	LT	10 mT-275°C	N	316.6	74.2	6	36.2	No origin-trending HT component
W025g.4	HT	100-300°C	Y	13.1	72	6	13.6	Inhomogeneous with subsample g.2; Weak moment
W025h.2	LC	NRM-6 mT	N	208.8	-5.9	4	9.6	
	LT	6 mT-200°C	N	30.1	-2.6	6	17.7	No origin-trending HT component

W025h.3	LC	NRM-10 mT	N	77.3	-3	6	22.5	No origin-trending HT component
W025i.2	LT	4 mT-325°C	N	118.1	35.1	11	15.3	
	HT	325-450°C	Y	270	-36	4	28.7	Not present in subsample i.3
W025i.3	LC	NRM-6 mT	N	69.6	-74.6	4	1.8	
	LT	6 mT-200°C	N	98.7	-37.3	6	9.7	
	MT	250-350°C	N	112.1	44.9	5	20.8	No origin-trending HT component
W025j.1	HT	8 mT-400°C	Y	95.8	18.1	11	2.1	
W025j.2	HT	100-350°C	Y	96.3	18.5	8	2.8	
W025j clast mean	HT			96	18.3	2	1.4	Mean of subsamples 1 and 2
W025k.3	HT	6 mT-560°C	Y	272.7	-22.9	20	8.9	
W025k.4	HT	6 mT-580°C	Y	270.5	-25.5	22	12.2	
W025k clast mean	HT			271.6	-24.2	2	7.2	Mean of subsamples 3 and 4
W025l.1	LC	NRM-10 mT	N	319	-31	6	7.2	
	HT	10 mT-300°C	Y	347.1	-43.1	7	5.6	
W025l.2	LT	4 mT-100°C	N	3.6	-36.1	5	0.9	
	MT	100-325°C	N	352.9	-36.9	7	16.9	
	HT	325-640°C	Y	331.7	-31.4	18	21.3	Hematite carrier
W025l clast mean				350.1	-40.1	2		Combining HT for subsample 1 with MT for subsample 2
W026.4	HT	4 mT-300°C	Y	30.3	-46.5	10	4.7	
W026.5	HT	4 mT-300°C	Y	36.1	-60.9	10	13.8	
W026 clast mean	HT			32.7	-53.7	2	32.8	Mean of subsamples 4 and 5

Note: The first column gives the sample name (samples with the same name before the period are from the same block/clast), the second column lists the component name, the third column lists the coercivity range or blocking temperature range, the fourth column denotes whether the PCA fit was anchored to the origin, the fifth column gives the declination, the six column gives the inclination, the seventh column gives the number of samples, the eighth column gives the maximum angular deviation (for individual fits) or 95% confidence intervals (for the means), and the final column gives notes and estimated Fisher *k* precision parameters. For all samples except fold test samples, inclination and declination are in geographic (i.e., in situ) coordinates. For fold test samples, top and bottom rows of inclination and declination give geographic and bedding-corrected coordinates, respectively. *Italicized* measurements were considered unreliable and are excluded from calculated mean values at the bottom of each subsection and from paleomagnetic field tests. All fits are line fits except for the great circle fit denoted by an asterisk (for which the pole location is listed in columns five and six).

Table S3. Peak unblocking temperatures for components oriented toward the Warakurna LIP local paleomagnetic field direction.

Sample	Lithology	Peak Temperature (°C)
BC0	dolerite	585
BC1	dolerite	585
Dol1	dolerite	560
Dol2	dolerite	530
Dol3	dolerite	585
Dol5	dolerite	530
D154d	dolerite	585
BCB2	quartzite near dolerite	510
BCB3	quartzite near dolerite	450
BCB4	quartzite near dolerite	575
BCB5	quartzite near dolerite	565
BCB6	quartzite near dolerite	520
BCB8	quartzite near dolerite	510
BCB10	quartzite near dolerite	575
BC3	quartzite near dolerite	225
BC4	quartzite near dolerite	585
BC6	quartzite near dolerite	565
BC7	quartzite near dolerite	570
BC8	quartzite near dolerite	560
BC9	quartzite near dolerite	560
BC10	quartzite near dolerite	360
D154c	quartzite near dolerite	500
D154e	quartzite near dolerite	565
D154f	quartzite near dolerite	520
D154g	quartzite near dolerite	560
D154h	quartzite near dolerite	225
D154i	quartzite near dolerite	320
D182a	monzogranite	290
D183	monzogranite	560
D184	monzogranite	575
D185	monzogranite	480
D186	monzogranite	540
D187	monzogranite	540
D188	monzogranite	320
Blob4a	monzogranite	520
Blob5b	monzogranite	520
Blob5c	monzogranite	520
D192b	quartzitic rock distal to dyke	360
D194c	quartzitic rock distal to dyke	520

D195a	quartzitic rock distal to dyke	360
D195b	quartzitic rock distal to dyke	320
D197a	quartzitic rock distal to dyke	350
D197b1	quartzitic rock distal to dyke	325
D197b2	quartzitic rock distal to dyke	325
D197c	quartzitic rock distal to dyke	325
D197d	quartzitic rock distal to dyke	350
EHJH5	Erawandoo Hill conglomerate clasts	345
EHJH5	Erawandoo conglomerate matrix	660
EHJH6	Erawandoo Hill conglomerate clasts	335
EHJH6	Erawandoo conglomerate matrix	335
EHJH7	Erawandoo Hill conglomerate clasts	>500
EHJH7	Erawandoo conglomerate matrix	450

Note: The first column gives the sample name, the second column lists the sample lithology, and the third column lists the peak unblocking temperatures of magnetization directions oriented like that of the local paleomagnetic field at 1070 Ma during the emplacement of the Warakurna LIP. When multiple subsamples of a given subsample were analyzed, the maximum unblocking temperature among the subsamples is shown here.

Supplementary References

Bowring, J.F., McLean, N.M., Bowring, S.A., 2011. Engineering cyber infrastructure for U-Pb geochronology: Tripoli and U-Pb_Redux. Geochem. Geophys. Geosyst. 12, Q0AA19.

Dunlop, D.J., Özdemir, O., 1997. Rock magnetism: Fundamentals and frontiers. Cambridge University Press, New York. 573 pp.

Dunlop, D.J., 2002. Theory and application of the Day plot (M_{rs}/M_s versus H_{cr}/H_c) - 1. Theoretical curves and tests using titanomagnetite data. J. Geophys. Res. 107, doi:10.1029/2001JB000486.

Jaffey, A.H., Flynn, K.F., Glendenin, L.E., Bentley, W.C., Essling, A.M., 1971. Precision measurement of half-lives and specific activities of ^{235}U and ^{238}U. Phys. Rev. C 4.

Li, H.-Y., Zhang, S.-H., 2005. Detection of mineralogical changes in pyrite using measurements of temperature-dependence suscpetibilities. Chinese Journal of Physics 48, 1454-1461.

Mattinson, J.M., 2005. Zircon U/Pb chemical abrasion (CA-TIMS) method; combined annealing and multi-step partial dissolution analysis for improved precision and accuracy of zircon ages. Chem. Geol. 220, 47-66.

McClean, N.M., Bowring, J.F., Bowring, S.A., 2011. An algorithm for U-Pb isotope dilution data reduction and uncertainty propagation. Geochem. Geophys. Geosyst. 12, Q0AA18.

Myers, J.S., 1995. The generation and assembly of an Archaean supercontinent: Evidence from the Yilgarn craton, Western Australia. J. Geol. Soc. London Spec. Pub. 95, 143-154.

Pidgeon, R.T., 1992. Recrystallisation of oscillatory zoned zircon: Some geochronological and petrological implications. Contrib. Mineral. Petrol. 110, 463-472.

Pidgeon, R.T., Wilde, S.A., 1998. The interpretation of complex zircon U–Pb systems in Archaean granitoids and gneisses from the Jack Hills, Narryer Gneiss Terrane, Western Australia. Precambrian Res. 91, 309-322.

Pidgeon, R.T., 2014. Zircon radiation damage ages. Chem. Geol. 367, 13-22.

Ramezani, J., Hoke, G.D., Fastovsky, D.E., Bowring, S.A., Therrien, F., Dworkin, S.I., Atchley, S.C., Nordt, L.C., 2011. High-precision U-Pb zircon geochronology of the Late Triassic Chinle Formation, Petrifi ed Forest National Park (Arizona, USA): Temporal constraints on the early evolution of dinosaurs. Geol. Soc. Am. Bull. 123, 2142–2159.

Rasmussen, B., Fletcher, I.R., Muhling, J.R., Wilde, S.A., 2010. In situ U–Th–Pb geochronology of monazite and xenotime from the Jack Hills belt: Implications for the age of deposition and metamorphism of Hadean zircons. Precambrian Res. 180, 26-46.

Rasmussen, B., Fletcher, I.R., Muhling, J.R., Gregory, C.J., Wilde, S.A., 2011. Metamorphic replacement of mineral inclusions in detrital zircon from Jack Hills, Australia: Implications for the Hadean Earth. Geology 39, 1143-1146.

Roberts, A.P., Cui, Y., Verosub, K.L., 1995. Wasp-waisted hysteresis loops: Mineral magnetic characteristics and discrimination of components in mixed magnetic systems. J. Geophys. Res. 100, 17909-17924.

Spaggiari, C.V., 2007. The Jack Hills greenstone belt, Western Australia Part 1: Structural and tectonic evolution over >1.5 Ga. Precambrian Res. 155, 204-228.
Spaggiari, C.V., Wartho, J.-A., Wilde, S.A., 2008. Proterozoic deformation in the northwest of the Archean Yilgarn Craton, Western Australia. Precambrian Res. 162, 354-384.
Tarduno, J.A., Cottrell, R.D., 2013. Signals from the ancient geodynamo: A paleomagnetic field test on the Jack Hills metaconglomerate. Earth Planet. Sci. Lett. 367, 123-132.
Tudryn, A., Tucholka, P., 2004. Magnetic monitoring of thermal alteration for natural pyrite and greigite. Acta Geophysica Polonica 52, 509-520.
Wang, L., Pan, Y.X., Li, J.H., Qin, H.F., 2008. Magnetic properties related to thermal treatment of pyrite. Science in China D 51, 1144-1153.
Wang, X.-C., Li, Z.-X., Li, J., Pisarevsky, S.A., Wingate, M.T.D., 2014. Genesis of the 1.21 Ga Marnda Moorn large igneous province byplume–lithosphere interaction. Precambrian Res. 241, 85-103.
Wingate, M.T.D., Pirajno, F., Morris, P.A., 2004. Warakurna large igneous province: A new Mesoproterozoic large igneous province in west-central Australia. Geology 32, 105-108.